

II Quantum electrodynamics

4 Feynman diagrams

We introduce the representation of subatomic particle interactions using Feynman diagrams. Richard Feynman invented these diagrams to provide intuition of the physical problem before commencing more detailed calculations. Here we also use their intuitive simplicity as a pedagogical tool to introduce central concepts in particle physics. We will first use them in the context of quantum electrodynamics (QED) is the microscopic theory of electromagnetism containing electrons, positrons, and photons.

4.1 Electromagnetic scattering

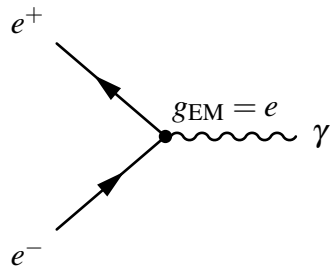
In QED, we represent matter (and fermions generally) with an arrowed solid straight line represents while a wiggly line represent photons (and spin-one bosons generally):

$$\longrightarrow = \text{electron} \quad (4.1)$$

$$\longleftarrow = \text{positron} \quad (4.2)$$

$$\sim = \text{photon} \quad (4.3)$$

We take the convention that electrons (matter) point to the right \rightarrow , and positrons (antimatter) point to the left \leftarrow . By themselves, these diagrams represent particles freely flying through space. Next, we represent the only interaction in QED by a vertex that may only connect two fermions with one photon:



$$(4.4)$$

This represents an interaction with strength set by the electromagnetic coupling $g_{\text{EM}} \propto e$, which is proportional to the electric charge e

$$g_{\text{EM}}^2 = \frac{e^2}{\epsilon_0 \hbar c} = 4\pi \alpha_{\text{EM}} \quad (4.5)$$

where α_{EM} is the fine structure constant. This is the small dimensionless real number

$$\alpha_{\text{EM}} = \frac{e^2}{4\pi \epsilon_0 \hbar c} \simeq \frac{1}{137} \simeq 0.0073. \quad (4.6)$$

The electric charge has the size $e = \sqrt{4\pi \alpha \epsilon_0 \hbar c}$, such that in natural Heaviside–Lorentz units $e = \sqrt{4\pi \alpha} \approx 0.3$.

More generally, a particle with multiplicative units of electric charge $Q_f e$ simple rescales the vertex factor

$$g_{\text{EM}} \rightarrow g_{\text{EM}} Q_f. \quad (4.7)$$

The QED vertex of equation (4.4) respects charge conservation: if one arrow goes into the vertex, the other arrow must leave. This is why I like to view the direction of the arrow in the straight line as a reminder of the flow of (negative) electric charge analogous to electric current in circuits. Historically, the literature likes to talk about positrons as negative energy states flowing backwards in time $Et \rightarrow (-E)(-t)$ called the Feynman–Stückelberg interpretation. Figure 24 shows the basic anatomy of a Feynman diagram representing an interaction via the exchange of a mediator.

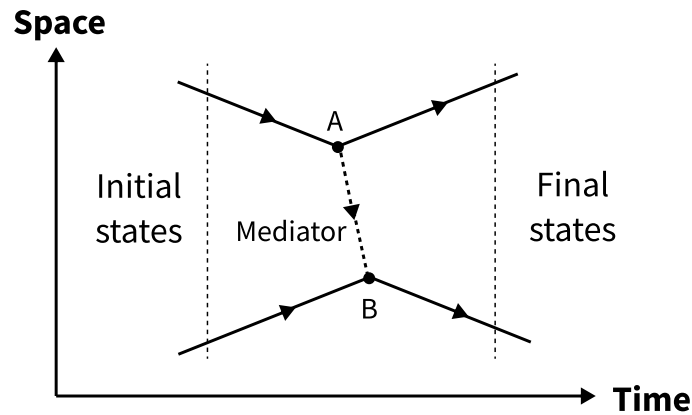


Figure 24: Schematic of Feynman diagram. Left shows two initial and and right shows two final states. An interaction is realised as the upper particle emits a mediator at vertex A, which is absorbed by the lower particle at vertex B.

With the basic ingredients of 4.3 and 4.4, we can draw the canonical interactions of quantum electrodynamics:

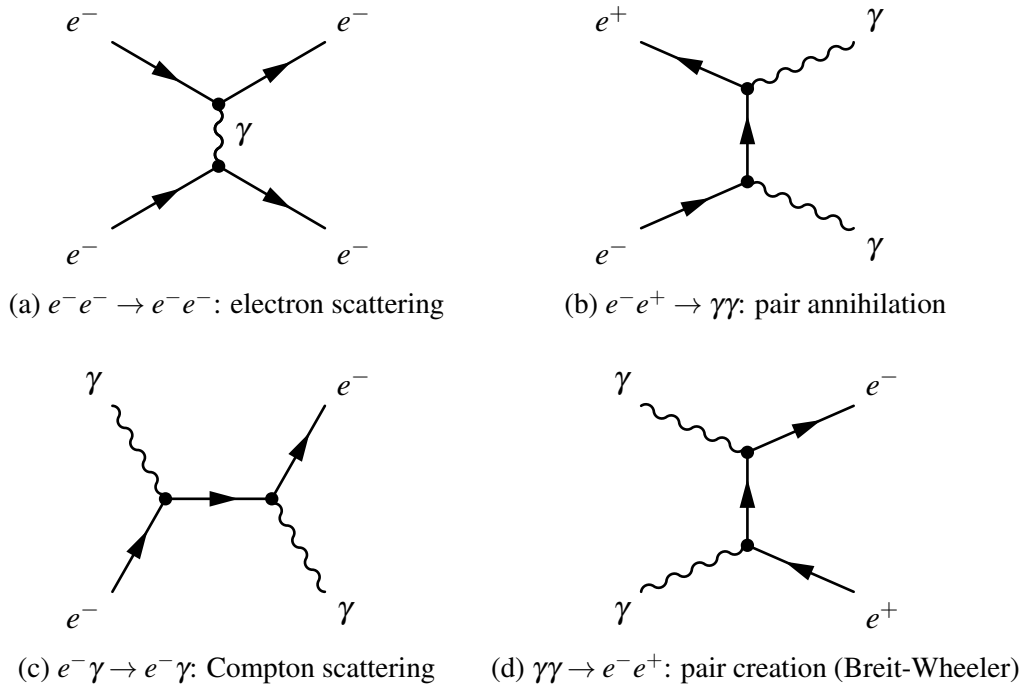


Figure 25: QED 2-to-2 scattering processes. This involves electrons, positrons and photons in quantum electrodynamics interacting via the fundamental QED vertex (4.4).

- Figure 25 shows various interactions involving electrons, positrons and photons: (25a) an electron e^- scattering off another electron via a virtual photon γ .
- Figure 25b an electron meeting a positron e^-e^+ and annihilating into two photons.
- Figure 25c shows Compton scattering where an electron scatters off a photon.
- Figure 25d shows the creation of an electron-positron pair from two photons. This is called the Breit–Wheeler process after Gregory Breit and John A. Wheeler studied this process in a Physical Review paper entitled “Collision of Two Light Quanta” [43] in 1934 while they both worked here at New York University. Today, I myself actively research this process alongside pair creation of other particles, namely $\gamma\gamma \rightarrow \mu\mu$ and $\gamma\gamma \rightarrow \tau\tau$ at the Large Hadron Collider.

We follow the common convention that places the initial states of a reaction on the left and final states on the right of a Feynman diagram.

4.2 Virtual particles

The exchange of virtual particles is the quantum mechanical description of force. Let us zoom into a particular Feynman diagram for closer analysis. Consider the interaction $1 + 2 \xrightarrow{X} 1' + 2'$:

$$\begin{array}{c} 1 \\ \swarrow \\ \text{---} \\ \searrow \\ 1' \end{array} \begin{array}{c} g_{1X} \\ \text{---} \\ X \\ \text{---} \\ g_{2X} \end{array} \begin{array}{c} \swarrow \\ 2 \\ \text{---} \\ \searrow \\ 2' \end{array} = \begin{array}{c} 1 \\ \swarrow \\ \text{---} \\ \searrow \\ 1' \end{array} \begin{array}{c} \text{---} \\ X \\ \text{---} \end{array} \begin{array}{c} \swarrow \\ 2 \\ \text{---} \\ \searrow \\ 2' \end{array} + \begin{array}{c} 1 \\ \swarrow \\ \text{---} \\ \searrow \\ 1' \end{array} \begin{array}{c} \text{---} \\ X \\ \text{---} \end{array} \begin{array}{c} \swarrow \\ 2 \\ \text{---} \\ \searrow \\ 2' \end{array} . \quad (4.8)$$

We describe X as a **virtual particle** that is **exchanged** because it does not appear in the final states. For time flowing left-to-right \rightarrow , the Feynman diagram is equal to the superposition of the two time-ordered diagrams on the right. It is momentarily created and annihilated at the vertices. In special relativity, we can work in the rest frame of particle 1 to conserve energy and momentum at the vertex g_{1X} , writing in four-momentum notation $\mathbf{P} = (E/c, \mathbf{p}) = (E, p_x, p_y, p_z)$:

$$\mathbf{P}_1 \rightarrow \mathbf{P}_{1'} + \mathbf{P}_X \quad (4.9)$$

$$\begin{pmatrix} m_1 \\ \mathbf{0} \end{pmatrix} \rightarrow \begin{pmatrix} E_1 \\ \mathbf{p}_1 \end{pmatrix} + \begin{pmatrix} E_X \\ -\mathbf{p}_1 \end{pmatrix}. \quad (4.10)$$

So the energies of particles 1 and X on the right-hand side are

$$E_1^2 = p_1^2 + (m_1)^2 \quad \text{and} \quad E_X^2 = p_1^2 + (m_X)^2$$

where $p_1 = |\mathbf{p}_1|$. Now consider the energy difference before and after the process at vertex g_{1X} :

$$\Delta E = (E_1 + E_X) - m_1 \rightarrow \begin{cases} 2p_1, & p_1 \gg m_1 \\ m_X, & p_1 \ll m_X \end{cases}.$$

We find $\Delta E \neq 0 \forall p_1$ meaning energy cannot be conserved at the vertex g_{1X} . This seems alarming, but we recall the energy–time uncertainty relation in quantum mechanics $\Delta E \Delta t \gtrsim \hbar$. This states that it is not possible to definitively know the precise energy of a system within a finite time. The “violation” of energy conservation is allowed for a duration of $\Delta t \leq \hbar/\Delta E$. Using $\Delta E \geq m_X$, we also infer the distance d for any exchange particle X to propagate before being absorbed by particle 2 is restricted by

$$d \leq R \equiv \frac{\hbar c}{m_X c^2}. \quad (4.11)$$

We define R as the **range** of the exchange particle and by implication the force. In general, 4-momentum need not be strictly conserved at a vertex. Note that for mass particles such as photons $m_X \rightarrow 0$, $R \rightarrow \infty$ implying infinite range for electromagnetism.

Mandelstam variables Particle physicists often adopt a notational conventional for any scattering of two initial and two final states (called **2-to-2 scattering**) to describe various momenta exchanged that are Lorentz invariant. Using the labels in figure 4.8, these are called the Mandelstam variables and defined as:

$$s = (P_1 + P_2)^2, \quad (4.12)$$

$$t = (P_1 - P_{1'})^2, \quad (4.13)$$

$$u = (P_1 - P_{2'})^2. \quad (4.14)$$

$$(4.15)$$

The \sqrt{s} equivalent to the centre-of-mass energy of the initial state system, and is widely used at particle accelerators. Meanwhile, \sqrt{t} is often seen when describing the momentum exchange.

4.3 Scattering and propagators

In quantum mechanics, we model interactions using potentials in the Hamiltonian of Schrödinger's equation. This allows us to calculate a matrix \mathcal{M} of final state $|f\rangle$ occurring due to a potential V given we start with initial state $|i\rangle$:

$$\mathcal{M}_{fi} = \langle f|V|i\rangle = \int \psi_f V \psi_i \mathbf{d}\mathbf{r}. \quad (4.16)$$

This has the heuristic:

$$\mathcal{M}_{fi} = |\text{prepare initial states}\rangle \rightarrow \boxed{\text{interaction happens}} \rightarrow |\text{measure final states}\rangle. \quad (4.17)$$

At this point, let us briefly review a selection of key results from scattering theory presented in non-relativistic quantum mechanics classes. Assuming the incident particle is a momentum eigenstate $|\phi\rangle = |\mathbf{k}\rangle$ of the free Hamiltonian $H_0 = \mathbf{k}^2/2m$. We can write this in position representation as a plane wave

$$\langle \mathbf{r}|\phi\rangle = \phi_0(\mathbf{r}) = \frac{1}{(2\pi)^{3/2}} e^{i\mathbf{k}\cdot\mathbf{r}} \quad (4.18)$$

normalised³⁵ by $(2\pi)^{3/2}$. We work with **sufficiently localised potentials** such that $V \rightarrow 0$ in the limit $|\mathbf{r}| \rightarrow \infty$. Quoting some results from standard quantum mechanics textbooks, the asymptotic solution to scattering off a potential $V(\mathbf{r})$ in three dimensions is a superposition of the incident plane and spherical waves scattered forward, denoted ψ_+ :

$$\psi(\mathbf{r}) \xrightarrow{r \rightarrow \infty} \phi_0(\mathbf{r}) + \psi_+(\mathbf{r}) = \frac{1}{(2\pi)^{3/2}} \left[e^{i\mathbf{k}\cdot\mathbf{r}} + f(\mathbf{k}', \mathbf{k}) \frac{e^{ikr}}{r} \right], \quad (4.19)$$

where r is the asymptotic observation position and $f(\mathbf{k}', \mathbf{k})$ is the **scattering amplitude**:

$$f(\mathbf{k}', \mathbf{k}) = -\frac{(2\pi)^3}{4\pi} 2m \langle \mathbf{k}'|V|\psi_+\rangle. \quad (4.20)$$

This $f(\mathbf{k}', \mathbf{k})$ contains all the information about the incident waves scattering off the potential V . In (4.19), we neglect the interference between the incident wave (first term) and the scattered spherical waves (second term).

We commonly work in the regime $H_0 \gg V$ where the kinetic energy of the incident beam dominates over the scattering potential. Then the scattering beam is, to a first approximation,

³⁵This slightly awkward normalisation will cause factors of $1/(2\pi)^3$ to appear in our Fourier transform like expressions going from space to momentum. This is sometimes known as the 'physicist' normalisation for Fourier transforms as opposed to the 'mathematician' $1/(2\pi)^{3/2}$ normalisation.

unchanged by V . So the final state of the system $|\psi_+\rangle$ is approximately equal to the initial momentum eigenstate $|\mathbf{k}\rangle$. It is possible to expand the scattering amplitude (4.20) as a Born series and keeping the leading term we have

$$f^{(1)}(\mathbf{k}', \mathbf{k}) = -\frac{(2\pi)^3}{4\pi} 2m \langle \mathbf{k}' | V | \mathbf{k} \rangle \quad (4.21)$$

So given a scattering potential V , we find the scattering amplitude $f^{(1)}(\mathbf{k}', \mathbf{k})$ is given by $f^{(1)}(\mathbf{k}', \mathbf{k}) \propto \langle \mathbf{k}' | V | \mathbf{k} \rangle$. Using the completeness relation $\int d^3\mathbf{r} |\mathbf{r}\rangle \langle \mathbf{r}|$ twice, we can recast (4.21) into the position representation:

$$\langle \mathbf{k}' | V | \mathbf{k} \rangle = \int d^3\mathbf{r}' \int d^3\mathbf{r} \langle \mathbf{k}' | \mathbf{r}' \rangle \langle \mathbf{r}' | V | \mathbf{r} \rangle \langle \mathbf{r} | \mathbf{k} \rangle = \int d^3\mathbf{r} \langle \mathbf{k}' | \mathbf{r} \rangle V(\mathbf{r}) \langle \mathbf{r} | \mathbf{k} \rangle, \quad (4.22)$$

where in the second equality, we apply a sufficiently localised potential $\langle \mathbf{r}' | V | \mathbf{r} \rangle = V(\mathbf{r}') \delta^{(3)}(\mathbf{r}' - \mathbf{r})$ such that integrating over the \mathbf{r}' sends $\mathbf{r}' \rightarrow \mathbf{r}$. Using the momentum eigenstates in position representation (4.18) we obtain

$$\langle \mathbf{k}' | V | \mathbf{k} \rangle = \frac{1}{(2\pi)^3} \int d^3\mathbf{r} V(\mathbf{r}) e^{i\mathbf{q}\cdot\mathbf{r}} \quad (4.23)$$

This is the central result of the **Born approximation**, which states that the scattering amplitude $f^{(1)}(\mathbf{k}', \mathbf{k})$ is proportional to the **Fourier transform of the scattering potential** $V(\mathbf{r})$ in momentum transfer space $\mathbf{q} \equiv \Delta\mathbf{k} = \mathbf{k} - \mathbf{k}'$. Recall from quantum mechanics that the probability current density formula is $\mathbf{j} = \frac{1}{2mi}(\psi^* \nabla \psi - \psi \nabla \psi^*)$. Applying this to (4.19), we find the differential cross-section is the modulus square of the scattering amplitude (4.20):

$$\frac{d\sigma}{d\Omega} = \frac{r^2 |\mathbf{j}^{\text{scat}}|}{|\mathbf{j}^{\text{inc}}|} = |f(\mathbf{k}', \mathbf{k})|^2. \quad (4.24)$$

This connects the theoretical scattering amplitude $f(\mathbf{k}', \mathbf{k})$ with an observable $d\sigma/d\Omega$. The interpretation of (4.24) is that $d\sigma$ is the probability incident particles are scattered into the solid angle element $d\Omega$. By performing scattering measurements of the differential cross-section (4.24), we can inverse Fourier transform to infer the scattering potential $V(\mathbf{r})$.

You may be feeling déjà-vu from optics classes? This because indeed you have seen the same effect as light or electrons passes through a single slit experiment (figure 26). The interference pattern $f(\mathbf{k})$ of wiggles you see on a screen far away from the slits is precisely the Fourier transform of the slit aperture $a(\mathbf{x})$

$$f(\mathbf{k}) \propto \int a(\mathbf{x}) e^{i\mathbf{k}\cdot(\mathbf{x}-\mathbf{x}')} d^3\mathbf{x}'. \quad (4.25)$$

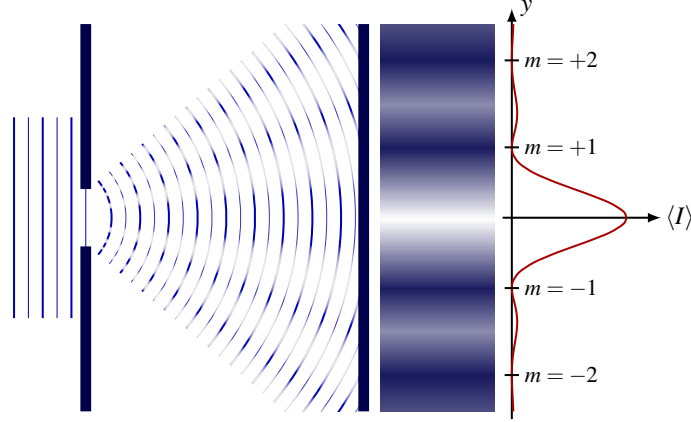


Figure 26: Diffraction pattern as Fourier transform. The interference pattern viewed far away by an observer is the Fourier transform of the aperture during waves scattering. In quantum mechanical scattering, the scattering amplitude is analogously the Fourier transform of the potential. Figure: tikz.net.

This is simply how waves behave! The wiggles encode all the information of ingoing waves interacting with the slits. In the quantum mechanical scattering, we have generalised the optical slits into any localised potential $V(r)$. This is actually how the path integral formulation of quantum mechanics works. As the slit width is taken to infinity, the amplitude is the sum of all possible paths taken.

We can model the range R of a force by adding an exponential function that decays rapidly $e^{-r/R}$ to a $1/r$ potential familiar from a classical Coulomb electrostatic force:

$$V_Y(r) = -\frac{g^2}{4\pi} \frac{e^{-r/R}}{r}. \quad (4.26)$$

We call this the **Yukawa potential**, after Hideki Yukawa who studied this for the strong nuclear force. Here, g is the coupling constant and R is the characteristic range of the potential according to (4.11). For those who enjoy multivariate calculus, we can align the momentum transfer \mathbf{q} in the z direction such that $\mathbf{q} \cdot \mathbf{r} = |\mathbf{q}|r \cos \theta$, we can perform the integral over spherical polar coordinates with $d^3\mathbf{r} = r^2 \sin \theta dr d\theta d\phi$:

$$\langle \mathbf{k}' | V_Y | \mathbf{k} \rangle = -\frac{1}{(2\pi)^3} \frac{g^2}{4\pi} \int_{r=0}^{\infty} \int_{\theta=0}^{\pi} \int_{\phi=0}^{2\pi} \frac{e^{-r/R}}{r} e^{i|\mathbf{q}|r \cos \theta} r^2 \sin \theta dr d\theta d\phi \quad (4.27)$$

To evaluate the angular parts of the integral, we can perform a change of variables $z = \cos \theta$, $dz = -\sin \theta d\theta$ to yield the radial integral

$$\langle \mathbf{k}' | V_Y | \mathbf{k} \rangle = -\frac{g^2}{(2\pi)^3} \frac{1}{2iq} \int_0^{\infty} \left[e^{(i|\mathbf{q}|-m_X)r} - e^{-(i|\mathbf{q}|-m_X)r} \right] dr. \quad (4.28)$$

Finishing this and overcoming some more algebra³⁶, the scattering amplitude becomes

$$\langle \mathbf{k}' | V_Y | \mathbf{k} \rangle = - \frac{g^2}{(2\pi)^3} \frac{1}{|\mathbf{q}|^2 + (m_X)^2}. \quad (4.29)$$

The coupling constant g parameterises the strength of the interaction. The two factors of g corresponds to the two vertices where the exchange particle X is created and annihilated. In general, for an amplitude calculation involving N vertices, there are N factors of g . Thus N is the **order** of the amplitude. We also identify the **propagator**:

$$- \frac{1}{|\mathbf{q}|^2 + (m_X)^2} \quad (4.30)$$

This represents the associated momentum and mass exchanged in the interaction. In relativistic formulations, this expression (4.30) generalises to the **relativistic Feynman propagator**:

$$\mathcal{P} = \frac{1}{Q^2 - (m_X)^2}, \quad (4.31)$$

where Q and m_X are the 4-momentum and invariant mass of the exchange particle X , respectively, involved in the interaction. For those taking quantum field theory, this is formally related to the Green's function $G(k)$ of the Klein–Gordon equation (3.36) in Fourier space:

$$(\square + m^2)G(x-y) = \delta(x-y) \quad \Rightarrow \quad (-k^2 + m^2)G(k) = 1. \quad (4.32)$$

We find that these virtual particles do not satisfy the usual P^2 relation:

$$Q^2 = E_X^2 - \mathbf{k}_X \cdot \mathbf{k}_X \neq (m_X)^2. \quad (4.33)$$

We call this inequality being **off mass-shell** and is required otherwise the propagator diverges. In general, the scattering amplitude of order N is related to the vertex factor gq_f and the propagator \mathcal{P} of the virtual exchange particle by:

$$\langle \mathbf{k}' | V | \mathbf{k} \rangle \propto \mathcal{M}_{fi} = \frac{(gq_f)^N}{Q^2 - (m_X)^2}. \quad (4.34)$$

For electromagnetic interactions, we need to calculate the amplitude $\langle f | V_{EM} | i \rangle$ where V_{EM} is the Coulomb potential. This is the Yukawa potential in the infinite range limit $R \rightarrow \infty$, or equivalently the mass of the mediator to zero $m_X \rightarrow 0$, as expected for massless photons.

³⁶Physically, we can invoke the far-distance argument, where the exponent vanishes $\lim_{r \rightarrow \infty} \exp[(i|\mathbf{q}| - m_X)r] \rightarrow 0$ in the $r \rightarrow \infty$ limit. The imaginary part of the argument causes oscillations while the real part exponentially decays as $r \rightarrow \infty$, implying no part of the exponent grows and we can therefore assume it vanishes in a physically sensible manner. For those who have taken complex analysis classes, a more rigorous treatment uses contour integrals to evaluate this in the complex plane and applies the residue theorem for each pole.

4.4 Gauge theory of electrodynamics

The quantum field theory classes cover this topic in far greater detail, but let us sketch out the main arguments for those not taking that course or for review. The gauge theory of electrodynamics is the simplest such theory of nature, and the prototype for generalisation to the strong and weak forces. From Maxwell’s equations (3.19), we can write the electromagnetic fields in terms of the electric ϕ and magnetic \mathbf{A} potentials as derivatives

$$\mathbf{E} = -\nabla\phi - \frac{\partial\mathbf{A}}{\partial t}, \quad \mathbf{B} = \nabla \times \mathbf{A}. \quad (4.35)$$

We can form the electromagnetic four-potential, which transforms as a four-vector

$$A^\mu = \begin{pmatrix} \phi \\ \mathbf{A} \end{pmatrix}. \quad (4.36)$$

The fields \mathbf{E}, \mathbf{B} remain invariant up to a gauge transformation to a function $\chi(x)$ whose space-time derivative exist

$$A^\mu \rightarrow A'^\mu = \begin{pmatrix} \phi - \partial_t \chi \\ \mathbf{A} + \nabla \chi \end{pmatrix}. \quad (4.37)$$

Electromagnetic fields remain invariant under such a transformation, which is a statement of **gauge invariance**. Recalling $A_\mu = \eta_{\mu\nu} A^\nu = \begin{pmatrix} \phi \\ -\mathbf{A} \end{pmatrix}$ and $\partial_\nu = \begin{pmatrix} \partial_t \\ +\nabla \end{pmatrix}$, we can write the gauge transformation in four-vector form as

$$A_\mu \rightarrow A'_\mu = A_\mu - \partial_\mu \chi(x). \quad (4.38)$$

In classical mechanics, we can define a Lagrangian $L(x, \dot{x}) = T - V$ for kinetic T and potential V energies such that Euler–Lagrange equation gives the equation of motion $\frac{\partial L}{\partial x} = \frac{d}{dt} \frac{\partial L}{\partial \dot{x}}$. It turns out we can extend this formalism to describe classical fields $\psi(x_\mu)$ that manifestly respect Lorentz invariance. We do this with a Lagrangian³⁷ $\mathcal{L}(\psi, \partial_\mu \psi) = \mathcal{T} - \mathcal{V}$ by identifying $x \rightarrow \psi(x_\mu)$ and its four-derivative $\dot{x} \rightarrow \partial_\mu \psi$ and applying the Euler–Lagrange equation yields the equation of motion

$$\frac{\partial \mathcal{L}}{\partial \psi} = \partial_\mu \left(\frac{\partial \mathcal{L}}{\partial (\partial_\mu \psi)} \right). \quad (4.39)$$

This is a ridiculously quick review of field theory, where further details about how this is quantised appears in Quantum Field Theory classes and textbooks.

³⁷Technically \mathcal{L} is the Lagrangian density $L = \int d^4x \mathcal{L}$ but textbooks often drop “density” for brevity.

The Dirac equation of motion (3.48) is given by to the Lagrangian

$$\mathcal{L}_{\text{Dirac}} = \bar{\psi}(i\gamma^\mu \partial_\mu - m)\psi. \quad (4.40)$$

The minimal coupling prescription of spin-half particles interacting with electromagnetism promotes the partial derivative in the Dirac equation to a **covariant derivative**:

$$\partial_\mu \rightarrow D_\mu = \partial_\mu + ieA_\mu. \quad (4.41)$$

So the Dirac Lagrangian becomes:

$$\mathcal{L} = \bar{\psi}(i\gamma^\mu D_\mu - m)\psi. \quad (4.42)$$

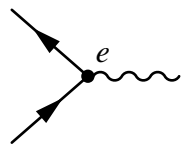
The Lagrangian (4.42) is invariant under a global complex phase. Mathematically, we see this with the transformation

$$\psi \rightarrow \psi' = \psi(x)e^{-i\alpha}, \quad \text{global U(1)} \quad (4.43)$$

where α is a constant and the Lagrangian remains invariant because the $\bar{\psi}$ introduces a factor of $e^{+i\alpha}$. We call this a **global U(1) symmetry** of Dirac theory. This is a continuous symmetry so by Emmy Noether's theorem³⁸, there is a conserved current

$$j^\mu = \bar{\psi}\gamma^\mu\psi. \quad (4.44)$$

This spinor current j^μ couples to the electromagnetic field A_μ in the covariant derivative leading to the QED interaction vertex:



$$= ieA_\mu j^\mu = ieA_\mu \bar{\psi}\gamma^\mu\psi. \quad (4.45)$$

Now let us change the global complex phase into a local complex phase such that it depends on spacetime $\alpha \rightarrow \alpha(x)$

$$\psi \rightarrow \psi' = \psi(x)e^{-i\alpha(x)}, \quad \text{local U(1)}. \quad (4.46)$$

³⁸For field theorists among our readers, this is technically a slightly stronger requirement that there is a symmetry of the action $S = \int d^4x \mathcal{L}_{\text{Dirac}}$, where $\mathcal{L}_{\text{Dirac}} = \bar{\psi}(i\gamma^\mu D_\mu - m)\psi$ is the Dirac Lagrangian. In this case, this global U(1) symmetry exists for the equation of motion, Lagrangian, and action.

We call this a **local U(1) transformation**. As the exponent is now a function of spacetime, the product rule applies for the derivative so the Dirac equation becomes

$$(i\gamma^\mu D_\mu - m)\psi \rightarrow [i\gamma^\mu (\partial_\mu - \underbrace{i\partial_\mu \alpha}_{\text{extra}} + ieA_\mu) - m]\psi'. \quad (4.47)$$

We now see this seems to have lost the U(1) symmetry due to the extra piece $i\partial_\mu \alpha(x)$ from the product rule.

But worry not, we can restore the invariance via the gauge transformation of the photon field (4.38): $A_\mu \rightarrow A'_\mu = A_\mu - \partial_\mu \chi(x)$. If we perform the local U(1) transformation on $\psi \rightarrow \psi e^{-i\alpha(x)}$ and gauge transformation $A_\mu \rightarrow A_\mu + \partial_\mu \chi(x)$ *simultaneously*, we can restore the invariance of the Dirac equation by identifying

$$\chi(x) = \frac{\alpha(x)}{e}. \quad (4.48)$$

So now we can state equation (4.42) is invariant under the simultaneous transformations:

$$\psi \rightarrow \psi e^{-i\alpha(x)}, \quad \text{local U(1) transformation,} \quad (4.49)$$

$$A^\mu \rightarrow A^\mu - \frac{1}{e} \partial^\mu \alpha(x), \quad \text{gauge transformation.} \quad (4.50)$$

This is the gauge theory of electromagnetism. Its mathematical simplicity belies its profundity that forces are deeply intertwined with local spacetime and gauge symmetries. By itself, embedding the two \pm physical polarisations of the photon ε_\pm into the four degrees of freedom of a Lorentz vector A_μ results in gauge redundancy.

However, in quantum mechanics, the potential A_μ seems more fundamental, which is what that couples to the complex phase of particle amplitudes. Figure 27 shows an electron traversing spacetime. Its wavefunction ψ acquires a complex phase that changes with its position and time, which is determined by the gauge freedom of the electromagnetic potential A_μ . In the case of U(1) electromagnetism, the phase traces out a circle, which is sometimes called the internal space. This is a manifestation of the Aharonov–Bohm effect, which is an experimental demonstration that a non-zero potential A_μ imparts a phase shift to the wavefunction even when the fields (first derivative of potentials) are zero.

The electromagnetic field strength tensor is given by

$$F^{\mu\nu} = \partial^\mu A^\nu - \partial^\nu A^\mu. \quad (4.51)$$

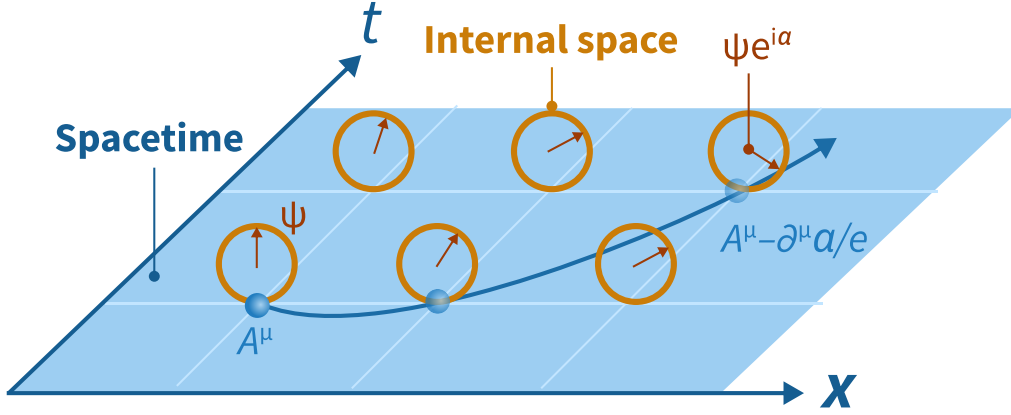


Figure 27: Sketch of gauge theory. A particle moving through spacetime in the presence of a non-trivial vector potential A^μ . The wavefunction acquires a change in local phase $\psi \rightarrow \psi e^{-i\alpha(x)}$, whose internal space of U(1) electromagnetism is a circle. The phase change corresponds to a change in the gauge potential $A^\mu \rightarrow A^\mu - \frac{1}{e} \partial^\mu \alpha$.

It is a traceless antisymmetric object that transforms as a tensor $F'^{\mu\nu} = \Lambda_\rho^\mu \Lambda_\sigma^\nu F^{\rho\sigma}$. We can write out in time-space coordinates in terms of the electric \mathbf{E} and magnetic \mathbf{B} fields as:

$$F^{\mu\nu} = \begin{pmatrix} 0 & -E_x & -E_y & -E_z \\ E_x & 0 & -B_z & B_y \\ E_y & B_z & 0 & -B_x \\ E_z & -B_y & -B_x & 0 \end{pmatrix}. \quad (4.52)$$

The field tensor $F^{\mu\nu}$ is gauge invariant by construction i.e. is invariant under a gauge transformation (4.50). The inhomogeneous Maxwell equations, namely Gauss' and Ampère's laws, in the presence of sources j_ν is written in manifestly covariant form as

$$\partial_\mu F^{\mu\nu} = j^\nu. \quad (4.53)$$

The source-free Maxwell equations are then written as

$$\partial_\mu F^{\mu\nu} = \square A^\nu - \partial^\nu (\partial_\mu A^\mu) = 0. \quad (4.54)$$

The Lagrangian that produces this equation of motion upon applying the Euler–Lagrange equation is

$$\mathcal{L}_{\text{Maxwell}} = -\frac{1}{4} F_{\mu\nu} F^{\mu\nu}. \quad (4.55)$$

The homogeneous Maxwell equations (no magnetic monopoles and Faraday's law) are captured by the Bianchi identity $\partial_\mu F_{\nu\sigma} + \partial_\nu F_{\sigma\mu} + \partial_\sigma F_{\mu\nu} = 0$. Combining the Maxwell and Dirac Lagrangian (4.42) gives

$$\mathcal{L}_{\text{QED}} = -\frac{1}{4}F_{\mu\nu}F^{\mu\nu} + \bar{\psi}(i\gamma^\mu D_\mu - m)\psi. \quad (4.56)$$

This is the Lagrangian for the theory of quantum electrodynamics. It is a marvel that this is our most precise description of electromagnetism and the prototype for the nuclear forces in the Standard Model.

Gauge fixing

We are always free to *choose* A^μ to satisfy the **Lorenz³⁹ gauge**

$$\partial_\mu A^\mu = 0. \quad (4.57)$$

To see this, say we acquired a gauge field A^μ that instead satisfies

$$\partial_\mu A^\mu = f(x), \quad (4.58)$$

where $f(x)$ is some non-zero well-behaved function. We are always free to perform a gauge transformation (4.50) to yield

$$\partial_\mu A^\mu - \square\chi = f(x). \quad (4.59)$$

If we wish to recover the Lorenz gauge $\partial_\mu A^\mu = 0$, we require this condition to hold:

$$\square\chi = -f(x). \quad (4.60)$$

This is the inhomogeneous wave equation which may always be solved for solutions. Hence we are always free to choose the Lorenz gauge.

In the Lorenz gauge, Maxwell's equations (4.54) reduce to a wave equation

$$\square A^\mu = 0, \quad (4.61)$$

³⁹This is named after Ludvig Lorenz (1829–1891), not Hendrik Lorentz (1853–1928) of the Lorentz transformations. Sometimes the literature calls this the 'Lorentz' gauge. Unfortunate misattribution aside, it is indeed a Lorenz covariant choice. Even worse, the pair have a Lorenz-Lorentz equation named after them. All this is not to be confused with Edward Lorenz (1917–2008) of the Lorenz attractor, pioneer of chaos theory.

which has solutions of the form

$$A^\mu = \int \frac{d^4k}{(2\pi)^4} \varepsilon^\mu(k) e^{-ik \cdot x}. \quad (4.62)$$

This has the form of a massless Klein–Gordon equation so analogous to (4.31), the relativistic photon propagator is simply

$$\mathcal{P} = \frac{1}{k^2}. \quad (4.63)$$

All our wonderful mathematics seem to imply the free electromagnetic field has four degrees of freedom. We know that there are two polarisations of free electromagnetic waves. There must be two constraints to ground us back to reality:

1. Choose (Lorenz) gauge

In (4.62) ε^μ is the **polarisation vector**. The Lorenz gauge (4.57) now becomes a statement of 4-orthogonality:

$$k_\mu \varepsilon^\mu = 0. \quad (4.64)$$

This now fixes one component of ε^μ in terms of the other three. For example, given our vectors are

$$k^\mu = \begin{pmatrix} k^0 \\ \mathbf{k} \end{pmatrix}, \quad \varepsilon^\mu = \begin{pmatrix} \varepsilon^0 \\ \boldsymbol{\varepsilon} \end{pmatrix}, \quad (4.65)$$

the timelike component is completely determined by the spacelike ones:

$$k_0 \varepsilon^0 = \mathbf{k} \cdot \boldsymbol{\varepsilon}. \quad (4.66)$$

We are down to 3 spatial independent components of ε^μ . One more to go.

2. Fix residual gauge freedom

Gauge freedom (4.50) in Fourier space becomes

$$A^\mu \rightarrow \tilde{A}^\mu = A^\mu + a k^\mu, \quad (4.67)$$

where a is some scalar. From (4.62) corresponds to the polarisation vector being defined up to scalar multiple of k^μ i.e. we can take

$$\varepsilon^\mu \rightarrow \tilde{\varepsilon}^\mu = \varepsilon^\mu + a k^\mu \quad (4.68)$$

This still satisfies the gauge condition (4.64) because $k^\mu k_\mu = 0$ for free fields. As we are free to add multiples of k^μ to ε^μ , let us choose $a = -\varepsilon^0/k^0$ such that the timelike

component of our redefined polarisation vector vanishes $\epsilon^0 = 0$. Then we obtain a statement of 3-orthogonality in the spatial degrees of freedom:

$$\mathbf{k} \cdot \boldsymbol{\epsilon} = 0. \quad (4.69)$$

This is in fact equivalent to imposing the **Coulomb gauge** $\nabla \cdot \mathbf{A} = 0$. **There are thus only two independent components of $\boldsymbol{\epsilon}$ perpendicular to \mathbf{k} .**

Without loss of generality we can align our z axis along the momentum of our electromagnetic wave, allowing us to choose k^μ and our two polarisation vectors $\epsilon_{1,2}^\mu$ to be

$$k^\mu = \begin{pmatrix} k^0 \\ 0 \\ 0 \\ k^0 \end{pmatrix}, \quad \epsilon_1^\mu = \begin{pmatrix} 0 \\ 1 \\ 0 \\ 0 \end{pmatrix}, \quad \epsilon_2^\mu = \begin{pmatrix} 0 \\ 0 \\ 1 \\ 0 \end{pmatrix}. \quad (4.70)$$

This is equivalent to vertical and horizontal polarised photons. One could also choose circular polarised photons

$$\epsilon_1^\mu = \frac{1}{\sqrt{2}} \begin{pmatrix} 0 \\ 1 \\ i \\ 0 \end{pmatrix}, \quad \epsilon_2^\mu = \frac{1}{\sqrt{2}} \begin{pmatrix} 0 \\ 1 \\ -i \\ 0 \end{pmatrix}. \quad (4.71)$$

The polarisation vectors satisfy the orthonormality condition:

$$\boldsymbol{\epsilon}_\lambda \cdot \boldsymbol{\epsilon}_{\lambda'} = \delta_{\lambda\lambda'} \quad \Leftrightarrow \quad (\epsilon_\lambda)^\mu (\epsilon_{\lambda'})_\mu = -\delta_{\lambda\lambda'}. \quad (4.72)$$

Finally the full Fourier decomposition of A^μ is

$$A^\mu(x) = \int \frac{d^3k}{(2\pi)^3 2E_{\mathbf{k}}} \sum_{\lambda=1}^2 \left[a_{\mathbf{k},\lambda} \epsilon_\lambda^\mu(\mathbf{k}) e^{-ik \cdot x} + a_{\mathbf{k},\lambda}^* \epsilon_\lambda^\mu(\mathbf{k}) e^{-ik \cdot x} \right] \quad (4.73)$$

These are the plane wave solutions, showing the photon as a superposition of the two polarisation states $\lambda = 1, 2$ over all available momenta \mathbf{k} .

QED Feynman rules

A class in particle physics would not be complete without stating some Feynman rules. These are algorithms for calculating a cross-section or decay, which are usually derived in QFT

classes. You can look these up in textbooks and for completeness, let us print them here. For on-shell initial and final states, we have:

$$e^- \longrightarrow \bullet = u(\mathbf{p}) \qquad e^- \bullet \longrightarrow = \bar{u}(\mathbf{p}) \qquad (4.74)$$

$$e^+ \longleftarrow \bullet = v(\mathbf{p}) \qquad e^+ \bullet \longleftarrow = \bar{v}(\mathbf{p}) \qquad (4.75)$$

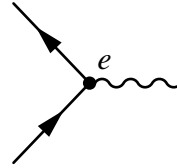
$$\gamma \text{ wavy line } \bullet = \varepsilon_\mu \qquad \gamma \bullet \text{ wavy line } = \varepsilon_\mu^* \qquad (4.76)$$

For off-shell internal lines denoted by *, the propagators are

$$e^* \bullet \longrightarrow \bullet = \frac{i(\gamma^\mu k_\mu + m)}{k^2 - m^2}, \qquad (4.77)$$

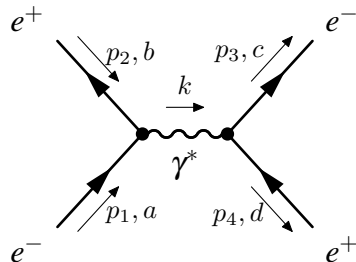
$$\gamma^* \bullet \text{ wavy line } \bullet = \frac{-i\eta_{\mu\nu}}{k^2}. \qquad (4.78)$$

The interaction vertex is the electric charge e :



$$= ie\gamma^\mu. \qquad (4.79)$$

Using these Feynman rules, we can draw Feynman diagrams then immediately write down the mathematical amplitude. As an example, Bhabba scattering involves $e^-e^+ \rightarrow e^-e^+$ for which an s-channel diagram is



$$\propto \underbrace{[\bar{v}^d(\mathbf{p}_4)(ie\gamma^\mu)u^c(\mathbf{p}_3)]}_{\text{outgoing}} \underbrace{\frac{\eta_{\mu\nu}}{(p_1 + p_2)^2}}_{\text{propagator}} \underbrace{[\bar{v}^a(\mathbf{p}_1)(ie\gamma^\nu)u^b(\mathbf{p}_2)]}_{\text{ingoing}}, \qquad (4.80)$$

where we apply momentum conservation for $k = p_1 + p_2$ and the letters a, b, c, d denote the spinor indices.

5 Scattering experiments

Scattering forms the experimental basis for studying particle physics. We just saw how to draw electromagnetic scattering processes as Feynman diagrams to represent the microscopic interaction. We now turn to connecting this to experiments of how we actually electrons and positrons to high energy before measuring how they interact. Typical experiments involve measuring the production rates of final states when a beam of particles is incident on a target.

5.1 Linear particle accelerators

Without realising it, the Crookes tubes used in the nineteenth century to study cathode rays constituted the first electron linear accelerators. The principle of a linear accelerator (linac) is to exploit the fact electric charges experience the Lorentz force and therefore accelerate in an electric field. Accelerating charged particles feel the Lorentz force

$$m \frac{d^2 \mathbf{x}}{dt^2} = \mathbf{f} = Q \left(\mathbf{E} + \frac{d\mathbf{x}}{dt} \times \mathbf{B} \right). \quad (5.1)$$

A motivation was Gamow's calculations that there is a finite probability of overcoming the Coulomb potential of a lithium nucleus using a proton into two helium nuclei:

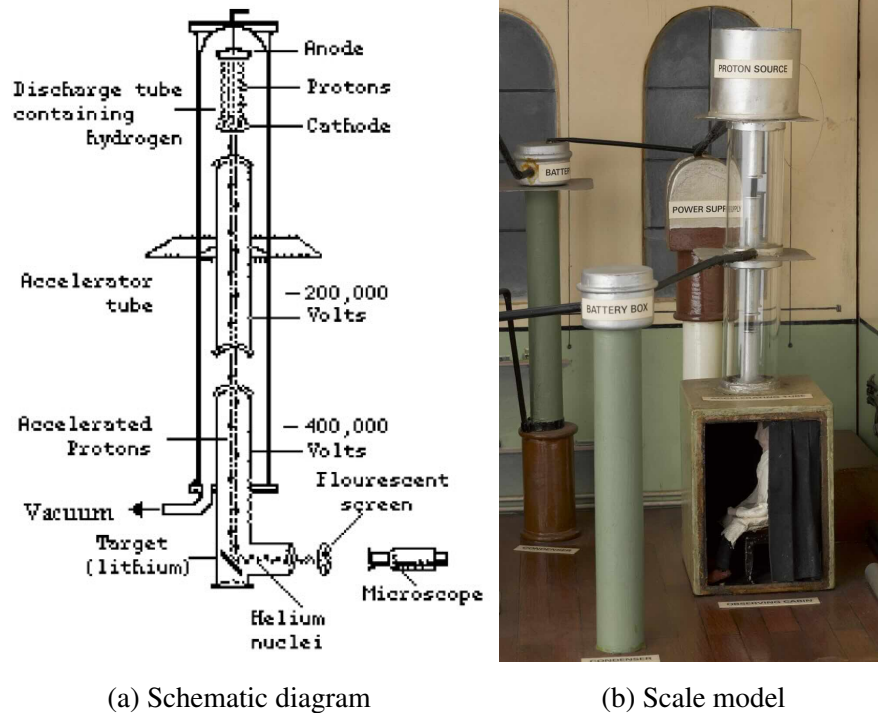


In 1932, John Cockcroft and Ernest Walton built the eponymous **Cockcroft–Walton generator** could accelerate protons up to 700 keV at the Cavendish Laboratory, Cambridge (figure 28a). This apparatus constituted the first linear accelerator of a hadron that reached sufficient energies above 150 keV to induce the artificial transmutation of atomic nuclei [44]. They were also able to test the energy–mass equivalence $E = mc^2$. Figure 28b shows a quaint model built for museum display of the original experiment at the Cavendish Laboratory ⁴⁰.

The key technological development was the voltage multiplier converting low-voltage alternating current into high-voltage direct current via a series of capacitors and diodes. This became a successful technology that was used by the likes of Fermilab and CERN as the initial stages of proton injection through the twentieth century (figure 29b). A contemporaneous device was the van der Graff generator.

Another major development is the **drift tube linac** (figure 30). Inside a vacuum drift tube, a series of cylindrical tubes establishes a series of uniform electric field between each

⁴⁰A wonderful photograph of Walton himself sitting in the viewing chamber is available here: <https://cudl.lib.cam.ac.uk/view/PH-CAVENDISH-P-00557/1>



(a) Schematic diagram

(b) Scale model

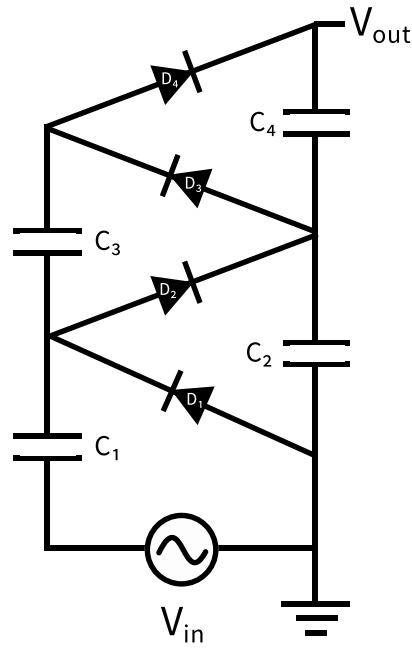
Figure 28: Cockroft–Walton accelerator apparatus. The first linear accelerator of protons was constructed in 1932 at Cambridge University and used in the first artificial transmutation of atomic nuclei. Images: [Fermilab](#), [Science Museum/W Lamprey](#).

tube. The injected charged particle, here an electron e^- , experiences a force $\mathbf{f} = e\mathbf{E}$ and accelerates between the tubes.

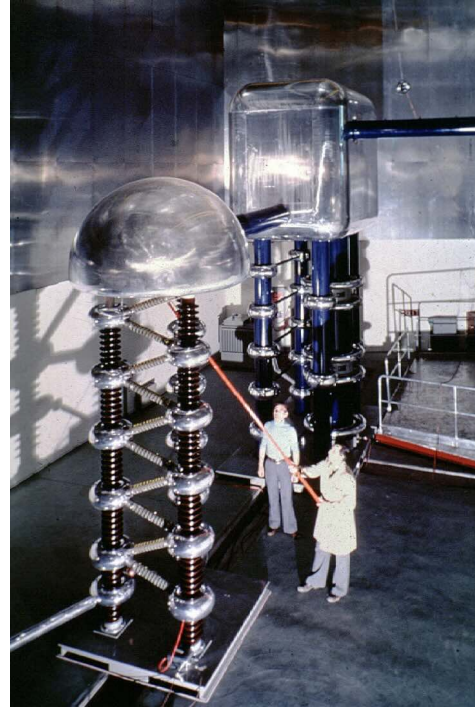
When the electron exits the first tube, a radio frequency driver generating a square wave inverts the voltage polarity of all tubes $\pm V \rightarrow \mp V$. This ensures the force vector always points in the same direction so the particle keeps accelerating.

If the polarity inversion were not synchronised to each electron exit, the electric field would decelerate the electron. We can then repeat this principle to accelerate beams up to very high energies and is highly efficient because the electron does not lose energy in any region. The main engineering limitations are a) producing large enough potential differences between each tube and b) constructing very long beamlines. Among the most powerful linear accelerator built is the Stanford Linear Accelerator (figure 31), which reaches two miles in length.

Rolf Widerøe developed the drift tube concept. For an oscillation frequency f of the driving oscillator, the length l_i of drift tube i , and β_i the velocity of the accelerated particle



(a) Voltage multiplier



(b) CERN CW multiplier

Figure 29: Cockroft–Walton (CW) voltage multiplier. (a) Crucial to reaching large voltages was the invention of the CW voltage multiplier scheme charging capacitors with an alternating current. (b) the 800 kV CW generator used until 1993 at CERN for pre-injection into the linear accelerator. Image: CERN [45].

when entering it, the condition that the particle remains in phase is established whenever

$$l_i = \frac{\beta_i c}{2f}. \quad (5.3)$$

5.2 Luminosity and cross-sections

To do science, we must use our theory to make measurable predictions. The cross-section is the most common observable in scattering experiments which justifies its study.

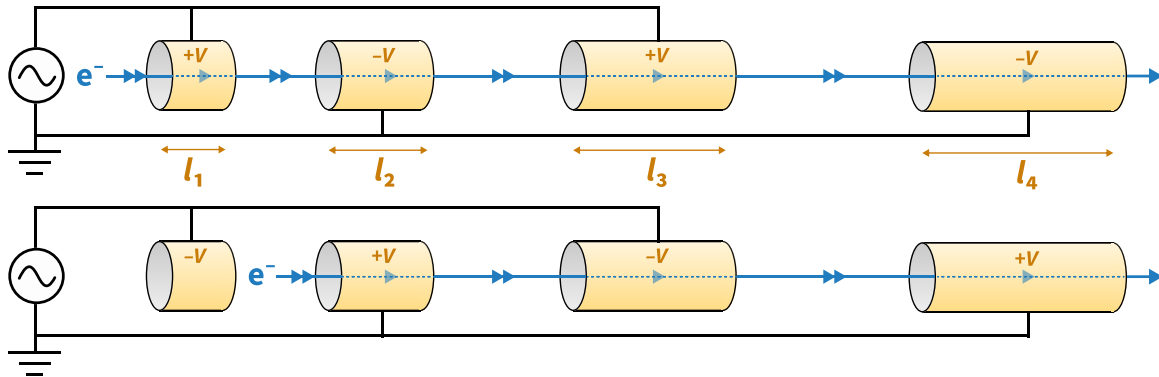


Figure 30: My cartoon of the drift tube linac concept. The injected particle accelerates outside the drift tubes wherein the particle traverses at constant velocity (single arrowhead). The acceleration region is in between the drift tubes (double arrowhead), which must increase in length l_i with increasing particle velocity. The lower sketch depicts the inverted polarity to ensure the particle accelerates in the same direction as before.

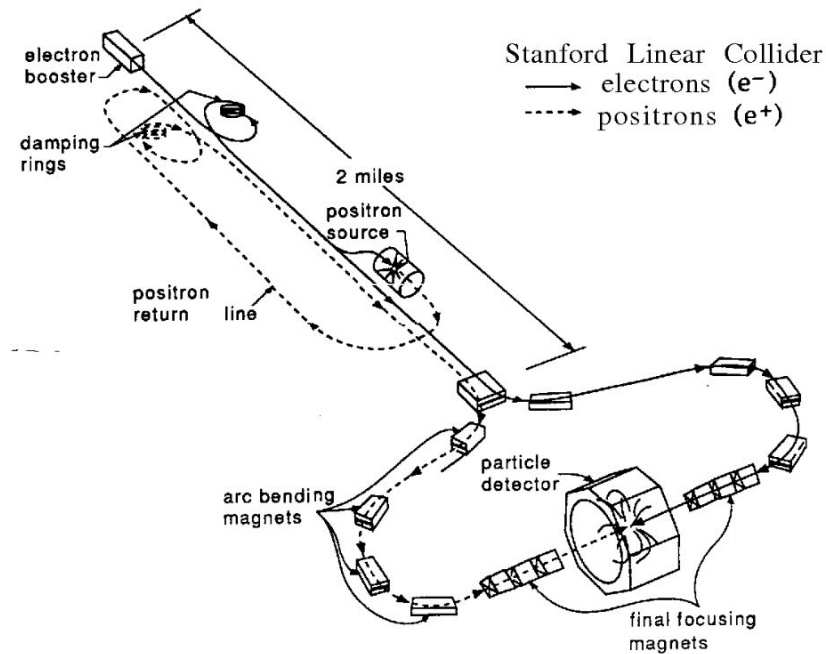
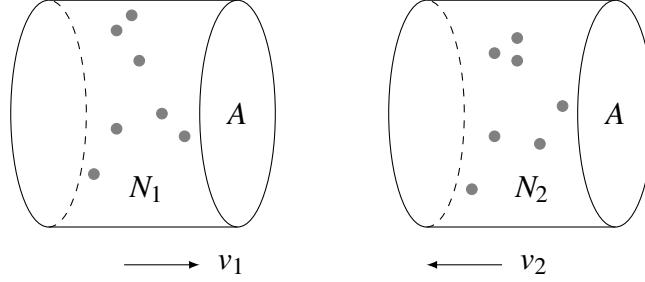


Figure 31: Stanford Linear Accelerator. This was the most powerful linear accelerator of electrons and positrons [46].

Particle accelerators have two beams that are aimed at each other:



The particle flux Φ of a beam is the number of particles per unit area per unit time

$$\Phi = n_i v_i = \frac{\dot{N}_i}{A} \quad (5.4)$$

- n_i : particle number density (number per unit volume) of incident beam,
- v_i : velocity of incident particles in beam,
- \dot{N}_i : rate of incident projectiles number per unit time,
- A : cross-sectional area of incident beam.

Given the incident beam illuminates N_t targets, the effective area of interaction is $S = N_t \sigma_r$, where σ_r is **cross-section** of the reaction r with rate w_r .

$$\sigma_r = \frac{w_r}{\Phi N_t}. \quad (5.5)$$

To obtain a better feel for this expression, rewrite this using (5.4):

$$w_r = \dot{N}_i N_t P_{\text{scat}}, \quad (5.6)$$

where $P_{\text{scat}} \equiv \sigma_r/A$ is interpreted as the scattering probability. So we see the reaction rate w_r is the rate of incident projectiles \dot{N}_i incident on N_t targets multiplied by the probability of interaction. Often we consider the number density of the targets n_t in some material of thickness x such that $N_t = n_t Ax$.

High-energy colliders use the term **instantaneous luminosity** for two colliding beams:

$$\mathcal{L} = \frac{\# \text{ particles crossing one another}}{\text{time interval} \times \text{unit transverse area}} = \frac{N_1 N_2}{\Delta t A}, \quad (5.7)$$

where $\Delta t = 1/f$ is the time interval (inverse frequency) between particle bunches, N_1 and N_2 are the number of particles in each bunch, and A is the transverse area of the beam. Accelerator physicists commonly use instantaneous luminosity with units of inverse area per unit time, where $\text{cm}^{-2} \text{s}^{-1}$.

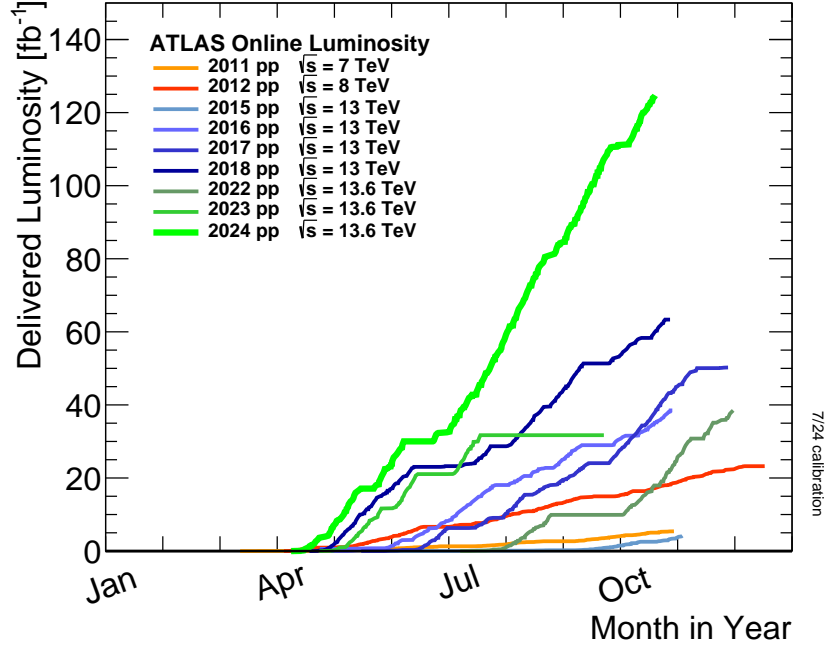


Figure 32: Integrated luminosity delivered to ATLAS Experiment. This shows the integrated luminosity $\int \mathcal{L} dt$ of the LHC delivered to ATLAS Experiment during different years. Figure: [ATLAS Luminosity Group](#).

The number of scattering events N_{events} is given by

$$N_{\text{events}} = \sigma \int \mathcal{L} dt, \quad (5.8)$$

where σ is the **total scattering cross-section** and instantaneous luminosity \mathcal{L} . We can also express this differentially in time as the **event rate** $R_{\text{events}} = \frac{dN_{\text{events}}}{dt}$. The experimental cross-section σ harbours all the physics of the interaction while \mathcal{L} is a machine parameter. As scattering cross-sections of elementary particles are tiny, particle physicists use the unit **barn**

$$1 \text{ barn} = 10^{15} \text{ fb} = 10^{-24} \text{ cm}^2. \quad (5.9)$$

The LHC has integrated luminosities reaching

$$L = \sigma \int \mathcal{L} dt = 10^{-34} \text{ cm}^{-2} \text{ s}^{-1} = 10 \text{ nb}^{-1} \text{ s}^{-1} \approx 100 \text{ fb}^{-1} \text{ year}^{-1}. \quad (5.10)$$

So the colloquialism “amount of data taken” in a year is usually expressed in units of inverse area fb^{-1} . The actual delivered luminosities to ATLAS are displayed in figure 32. So if there is an process that has a cross-section $\sigma = 20 \text{ fb}$, a machine delivering an integrated luminosity of $L = 100 \text{ fb}^{-1}$ would produce around $N = \sigma L = 2000$ events of that process.

5.3 Fermi's golden rule

This is a review of the standard non-relativistic derivation found in all quantum mechanics textbooks, which is sketched here for completeness. This applies time-dependent perturbation theory to model the time evolution of dynamics induced by a small perturbation. We start with the unperturbed Hamiltonian \hat{H}_0 and a small $\lambda \ll 1$ time dependent perturbation $\hat{H}_1(t)$ to give

$$\hat{H} = \hat{H}_0 + \lambda \hat{H}_{\text{int}}(t). \quad (5.11)$$

We can express the time dependent state $|\psi(t)\rangle$ as a linear superposition of the eigenstates of \hat{H}_0

$$|\psi(t)\rangle = \sum_n c_n(t) e^{-iE_n^{(0)}t} |n^{(0)}\rangle \quad (5.12)$$

Substituting this into the time-dependent Schrödinger equation $i\frac{d|\psi\rangle}{dt} = \hat{H}|\psi\rangle$ then multiplying through by the final state $\langle f^{(0)}|$ gives

$$\frac{dc_f}{dt} = \frac{1}{i} \sum_n c_n e^{i(E_f^{(0)} - E_n^{(0)})t} \langle f^{(0)} | \hat{H}_{\text{int}} | n^{(0)} \rangle. \quad (5.13)$$

We now approximate using perturbation theory by expanding c_n as a power series in λ : $c_n(t) = c_n^{(0)} + \lambda c_n^{(1)} + \dots$. Equating the first order terms gives the 1st order correction to the expansion coefficients

$$c_f^{(1)}(t) = \frac{1}{i} \sum_n c_n^{(0)} \int_{t_0}^t e^{i(E_f^{(0)} - E_n^{(0)})t'} \langle f^{(0)} | \hat{H}_{\text{int}} | n^{(0)} \rangle dt'. \quad (5.14)$$

Consider the case where at $t = 0$, the system is in the 'initial' state $|i\rangle$ such that $c_n^{(0)} = 1$ is non-zero only for $n = i$. Equation (5.14) becomes

$$c_f^{(1)}(t) = \frac{1}{i} \int_0^t e^{i\Delta E_{fi}t'} \langle f^{(0)} | \hat{H}_{\text{int}} | i^{(0)} \rangle dt', \quad (5.15)$$

where $\Delta E_{fi} \equiv E_f^{(0)} - E_i^{(0)}$. Evaluating the integral gives

$$c_f^{(1)}(t) = \frac{1}{i} \langle f^{(0)} | \hat{H}_{\text{int}} | i^{(0)} \rangle \frac{e^{i\Delta E_{fi}t} - 1}{i\Delta E_{fi}}. \quad (5.16)$$

Taking the modulus square of this gives the probability of transition from $|i^{(0)}\rangle$ to $|f^{(0)}\rangle$ due to the perturbation

$$P_{i \rightarrow f} = |c_f^{(1)}(t)|^2 = |\langle f^{(0)} | \hat{H}_{\text{int}} | i^{(0)} \rangle|^2 t^2 \text{sinc}^2 \left(\frac{\Delta E_{fi}t}{2} \right), \quad (5.17)$$

where $\text{sinc}(x) \equiv \sin(x)/x$. Let the perturbation induce a transition into a continuum set of final states $|f\rangle$ with a continuous energy spectrum $E_f \rightarrow E(p_f)$ where p_f is the momentum. The transition probability is as given by (5.17) integrating over the final continuum set of states

$$P_{i \rightarrow f} = \int_0^\infty |\langle f | \hat{H}_{\text{int}} | i \rangle|^2 t^2 \text{sinc}^2\left(\frac{\Delta E_f t}{2}\right) dp_f, \quad (5.18)$$

where $\text{sinc}(x) \equiv \sin(x)/x$. Changing variables of the argument of the sinc function

$$q = \frac{\Delta E_f t}{2}, \quad dq = \frac{dE(p_f)}{dp_f} dp_f \frac{t}{2}. \quad (5.19)$$

We introduce the **density of states**

$$\rho(E_f) = \frac{dp_f}{dE_f}, \quad (5.20)$$

which measures the quantity of continuum final states contained within $[p_f, p_f + dp_f]$ given an energy interval $[E_f, E_f + dE_f]$. We assume the transition amplitude $\langle f | \hat{H}_{\text{int}} | i \rangle$ occurs on a much faster timescale than measurements involving the time evolution of q so is effectively time-independent. We can therefore take $\langle f | \hat{H}_{\text{int}} | i \rangle$ out of the time integral and extend the limits to $\pm\infty$

$$P_{i \rightarrow f} \simeq 2t \rho(E_f) |\langle f | \hat{H}_{\text{int}} | i \rangle|^2 \int_{-\infty}^{\infty} \text{sinc}^2(q) dq. \quad (5.21)$$

The integral evaluates to π . Differentiating with respect to time gives the rate of transition probability to the continuum set of states

$$\boxed{\frac{dP_{i \rightarrow f}}{dt} = 2\pi \underbrace{|\langle f | \hat{H}_{\text{int}} | i \rangle|^2}_{\text{dynamics}} \underbrace{\rho(E_f)}_{\text{kinematics}}}. \quad (5.22)$$

This is the **Fermi golden rule**. This tells us the rate $w_{fi} = \frac{dP_{i \rightarrow f}}{dt}$ of an initial state $|i\rangle$ to transition into final state $|f\rangle$. The matrix element $\mathcal{M}_{fi} = \langle f | H_{\text{int}} | i \rangle$ captures the dynamics of the Hamiltonian H_{int} represented by Feynman diagrams, while $\rho(E_f)$ captures kinematics and is sometimes called *phase space*.

$$\left(\begin{array}{c} \text{Transition} \\ \text{rate} \end{array} \right) = 2\pi \times \left(\begin{array}{c} \text{Feynman} \\ \text{diagrams} \end{array} \right) \times \left(\begin{array}{c} \text{Phase} \\ \text{space} \end{array} \right). \quad (5.23)$$

This holds when the time scale for transition $|i\rangle \rightarrow |f\rangle$ is much faster than the measurement time and the interaction potential is weak compared to the kinetic energies of the incident particles.

The cross section is related to the transition probability divided by the flux factor Φ_{inc} of incident particles

$$\sigma = \frac{2\pi}{\Phi_{\text{inc}}} |\mathcal{M}_{fi}|^2 \rho(E_f). \quad (5.24)$$

Given particles in incident beams 1 and 2, we can write the Lorentz invariant (frame independent) flux factor in various forms

$$\Phi_{\text{inc}} = 2E_1 2E_2 |\mathbf{v}_1 - \mathbf{v}_2| \quad (5.25)$$

$$= 4\sqrt{(p_1 \cdot p_2)^2 - m_1^2 m_2^2} \quad (5.26)$$

$$= 2\sqrt{(s - m_1^2 - m_2^2)^2 - 4m_1^2 m_2^2}. \quad (5.27)$$

This simplifies for the cases of ultrarelativistic incident particles $s \gg m_{1,2}$. For fixed-target experiments with particle 2 at rest, this reduces to

$$\Phi_{\text{inc}}^{\text{fixed-target}} = 2E_1 2m_2 |\mathbf{v}_1|. \quad (5.28)$$

The cross-section for two particles colliding with energy E_1 and E_2 is,

$$\sigma_{12 \rightarrow X} = \frac{1}{2E_1 2E_2} \frac{1}{|\mathbf{v}_1 - \mathbf{v}_2|} 2\pi |\mathcal{M}_{fi}|^2 \rho(E_f). \quad (5.29)$$

In real experiments, a particle detector might only see a small solid angle of scattered events. Therefore, it is useful to define the **differential cross-section** $d\sigma_r/d\Omega$ for the number of events scattered into a particular solid angle $d\Omega = \sin\theta d\theta d\phi$ as:

$$\frac{dN}{d\Omega} = \frac{d\sigma_r(\theta, \phi)}{d\Omega} \times \int \mathcal{L} dt. \quad (5.30)$$

5.4 Density of states

We now study the study the density of states $\rho(E_f)$ in more detail. In non-relativistic quantum mechanics, textbooks consider a free particle with wavefunction $\psi(x) = Ne^{-i(Et - p_x x)}$ in a box of length L . Requiring the modulus square of the wavefunction to integrate to unity (to gives a probability) fixes the normalisation N :

$$\int_0^L \psi^* \psi dx = 1, \quad \Rightarrow \quad N = \frac{1}{\sqrt{L}}. \quad (5.31)$$

Periodic boundary conditions for a particle in a box $\psi(x+L) = \psi(x)$ implies $e^{ipx} = e^{ip(x+L)}$. Expressing unity as a periodic complex number $1 = e^{i(2\pi n)}$ for integer n , the momenta are quantised:

$$e^{i(pL)} = 1 = e^{i(2\pi n)}, \quad \Rightarrow \quad p_n = \frac{2\pi n}{L}. \quad (5.32)$$

We can then write how many states squished into the (infinitesimal) interval $[n, n + dn]$ have momentum $[p, p + dp]$ as

$$dn = \frac{dp}{2\pi} L. \quad (5.33)$$

In the final calculations, every final state particle will introduce a factor of $1/L$ in the matrix element squared $|\mathcal{M}_{fi}|^2$. This cancels with the L in the density of states factor, so we can henceforth drop the factors of L . Generalising this to the four dimensions of energy-momentum, we can write this in terms of the infinitesimal four-momentum space volume $d^4P = dE dp_x dp_y dp_z$

$$d^4n = \frac{d^4P}{(2\pi)^4}. \quad (5.34)$$

This turns out to be Lorentz invariant and many textbooks write this in a form with physical constraints, namely that the final-state particles are on their mass shell $P^2 = m^2$ imposed and they have positive mass $m > 0$. Formally, they do this by integrating over the energy component of the four-momentum $P^0 = E$ using a Dirac delta function⁴¹ $(2\pi)\delta(P^2 - m^2)$ for the on-mass-shell condition and a step function to enforce mass positivity⁴² $m > 0$, yielding:

$$d^3n = \frac{d^3\mathbf{p}}{(2\pi)^3} \int \frac{dE}{2\pi} (2\pi)\delta(P^2 - m^2) = \frac{d^3\mathbf{p}_f}{2E_f(2\pi)^3}. \quad (5.35)$$

We can perform the integral using a change of variables $x = E^2$, $dx = 2E dE$. Every final state particle with momentum \mathbf{p}_f comes with a factor of phase space and one set of delta functions (with factors of $(2\pi)^4$ for Fourier normalisation) to impose energy-momentum conservation $(2\pi)^4 \delta^{(4)}(\sum_f P_f - \sum_i P_i)$ momentum conservation:

$$d^{(3N)}n = (2\pi)^4 \delta^{(4)} \left[\sum_f P_f - \sum_i P_i \right] \prod_{f=1}^N \frac{d^3\mathbf{p}_f}{2E_f(2\pi)^3}, \quad (5.36)$$

where $P_{i(f)}$ are the initial-state (final-state) four-momenta. What is the physical meaning of all this? This tells us that the density of available states is related to the momentum available to the final states.

⁴¹The delta function is defined by $\int_{-\infty}^{\infty} \delta(x-a)f(x)dx = f(a)$ and $\int_{-\infty}^{\infty} \delta(x)dx = 1$.

⁴²The Heaviside step function is defined as $\Theta(m) = 1$ for $m > 0$, $\Theta(m) = 0$ for $m < 0$.

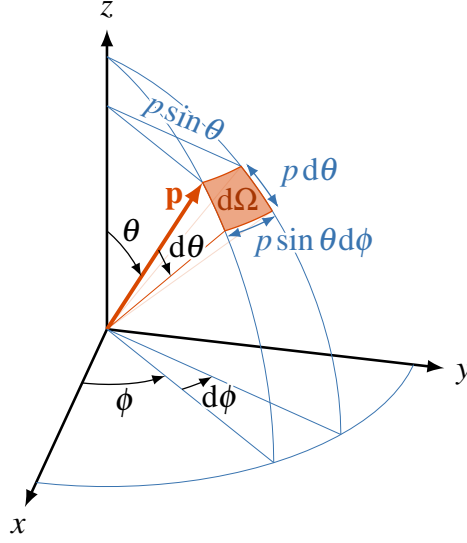


Figure 33: Spherical coordinates. Momentum expressed in spherical coordinates with infinitesimal angular elements $d^3\mathbf{p} = p^2 dp d\Omega$, where the solid angle is $d\Omega = \sin\theta d\theta d\phi$. Drawing adapted from [I. Neutelings](#).

Two body final state

We can calculate the density of states for the simplest case of two particles in the final state. Using the situation set up in figure 3.11, we have to write

$$dn = \frac{d^3\mathbf{p}_1}{2E_1(2\pi)^3} \frac{d^3\mathbf{p}_2}{2E_2(2\pi)^3} (2\pi)^4 \delta(E_1 + E_2 - E_{\text{CM}}) \delta^{(3)}(\mathbf{p}_1 + \mathbf{p}_2) \quad (5.37)$$

Integrating over $d^3\mathbf{p}_2$ imposes momentum conservation as the delta function fixes $\mathbf{p}_1 = -\mathbf{p}_2$. We denote this final-state momentum $\mathbf{p}_f = \mathbf{p}_1 = -\mathbf{p}_2$ with subscript f :

$$dn = \frac{1}{2E_1 2E_2} \frac{d^3\mathbf{p}_f}{(2\pi)^2} \delta(E_1 + E_2 - E_{\text{CM}}). \quad (5.38)$$

We now write $d^3\mathbf{p}_f$ in spherical coordinates $d^3\mathbf{p}_f = p_f^2 dp_f d\Omega$, where $p_f \equiv |\mathbf{p}_f|$ and $d\Omega$ is the solid angle visualised in figure 33. To help integrate the delta function, we perform the substitution $x = E_1 + E_2 - E_{\text{CM}}$ then use the chain rule because $E_a = E_a(p_f)$ is a function of p_f :

$$dx = \left(\frac{dE_1}{dp_f} + \frac{dE_2}{dp_f} \right) dp_f = \left(\frac{p_f}{E_1} + \frac{p_f}{E_2} \right) dp_f = \left(\frac{E_1 + E_2}{E_1 E_2} \right) p_f dp_f, \quad (5.39)$$

where the second equality differentiated the energy-momentum relation

$$E_a^2 = p_f^2 + m_a^2 \Rightarrow \frac{dE_a}{dp_f} = \frac{p_f}{E_a}. \quad (5.40)$$

We can now substitute dp_f from the change of variables (5.39) to convert equation (5.38) into an integral over x :

$$dn = \frac{1}{4} \frac{p_f}{E_1 + E_2} \frac{d\Omega}{(2\pi)^2} \delta(x) dx. \quad (5.41)$$

Performing the delta function integration enforces $x = 0 \Rightarrow E_1 + E_2 = E_{\text{CM}}$, yielding the two-body phase space expression:

$$\boxed{dn_{\text{two-body}} = \frac{1}{2} \frac{p_f}{E_{\text{CM}}} \frac{d\Omega}{(4\pi)^2}.} \quad (5.42)$$

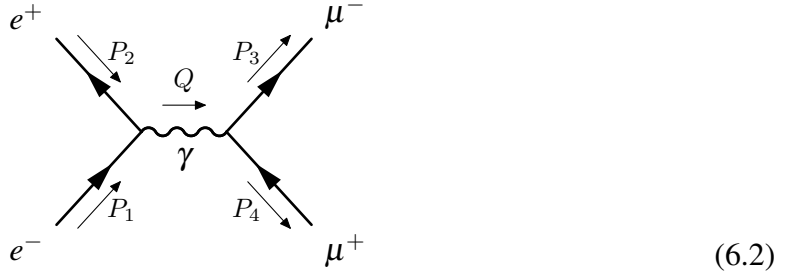
Given how often processes have two particles in the final state, this is a very useful result.

6 Electron–positron annihilation

We now illustrate all these concepts in a concrete and classic calculation of QED, the ‘hydrogen atom of particle physics’. This is electron–positron annihilation via the electromagnetic interaction to produce a muon–antimuon pair:

$$e^- e^+ \rightarrow \gamma \rightarrow \mu^- \mu^+. \quad (6.1)$$

The corresponding Feynman diagram with momenta labelled looks like this:



This is the only tree-level Feynman diagram for $e^- e^+ \rightarrow \mu^- \mu^+$, making it among the simplest QED process to calculate with high pedagogical value. Indeed we cannot write down a t-channel diagram that is possible for $e^- e^+ \rightarrow e^- e^+$ (figure 25a) because one QED vertex cannot change an electron to a muon (QED conserves flavour). Such calculations will nonetheless find renewed experimental importance at the highest energies in the coming decades because the likely successor to the Large Hadron Collider will be an $e^- e^+$ machine to study the Higgs boson precisely.

There are various techniques to calculate the quantum amplitude of figure 6.2. In QFT classes, you will likely learn Dirac gamma matrix algebra with spinor trace sum identities, which are powerful algorithms. However, we shall analyse the helicity amplitudes (e.g. Larkoski and Thomson textbooks) to expose the underlying physics. We take the ultra-relativistic limit $m \rightarrow 0$ from the outset and invoke various physical principles to further reduce the calculation to a handful of matrix multiplications that is tolerable with pen and paper.

Dimensional analysis prelude As usual in physics, it is useful to get a feeling for how the answer should depend on key physical quantities before commencing an extended calculation. First, we can work in the centre-of-mass frame to let the four-momenta of the electron, positron and (virtual) photon be

$$P_{e^-} = \begin{pmatrix} E_e \\ \mathbf{p} \end{pmatrix}, \quad P_{e^+} = \begin{pmatrix} E_e \\ -\mathbf{p} \end{pmatrix}, \quad Q_\gamma = P_{e^-} + P_{e^+} = \begin{pmatrix} 2E_e \\ \mathbf{0} \end{pmatrix}. \quad (6.3)$$

The cross-section (with dimensions length squared) must be proportional to the inverse square of centre-of-mass energy (given $(\hbar c)^2$ having units of length-energy squared). Meanwhile, we count there are two electromagnetic vertices in the Feynman diagram giving a factor of e^2 for the amplitude, which upon squaring gives $e^4 = (4\pi\alpha_{\text{EM}})^2$.

The Feynman diagram (figure 6.2) has 2 vertices involving particles of unit charge. The vertex factor is then

$$g_{\text{EM}}^2 = 4\pi\alpha_{\text{EM}}$$

The only scale in our system is the centre-of-mass energy, so we can write with the Mandelstam variable $s = E_{\text{CM}}^2 = (2E_e)^2$ and can assemble our dimensional analysis expectation

$$\sigma \propto \frac{\alpha_{\text{EM}}^2}{s}. \quad (6.4)$$

Remarkably, this by itself is only a factor of $4\pi/3$ different from the full calculation that account for all the flux, spin and phase space factors if you take a sneak peek ahead to equation (6.24).

We can also obtain the correct $(1 + \cos^2 \theta)$ angular dependence in the differential cross-section, by arguing the photon mediator means we can write the circular polarisation vectors $(0, i, \pm 1, 0)$ then performing a rotation in the polar angle.

6.1 Spinor-helicity analysis

Naïvely inspecting the process $e^- e^+ \rightarrow \mu^- \mu^+$, we see 4 distinct particles in the problem (electron, positron, muon, antimuon), each of which can have one of two charges $(+, -)$ and two helicities (L, R), giving 16 possible distinct combinations. Fortunately, we are physicists who can invoke the physical argument of angular momentum conservation to reduce this down to only four possibilities. The photon is spin 1, so the combination of spin for the initial and final states must also sum to 1 to respect angular momentum conservation. To see what these combinations are, we see forbidden combinations are those whose helicity states are in opposite directions:

$$e^- \xrightarrow{\text{R}} \mathbf{p} \quad -\mathbf{p} \xleftarrow{\text{R}} e^+ \quad \text{spin } 0 \Rightarrow \text{forbidden} \quad (6.5)$$

By contrast, these helicity states intuitively sums to spin one and is therefore allowed:

$$e^- \xrightarrow{\text{R}} \mathbf{p} \quad -\mathbf{p} \xleftarrow{\text{L}} e^+ \quad \text{spin } 1 \Rightarrow \text{allowed} \quad (6.6)$$

This applies to both initial and final states so the only allowed helicity combinations are ones where the particle-antiparticle pair have opposite helicity such that the spin sums to one:

$$\begin{aligned}
 e^- e^+ &\rightarrow \mu^- \mu^+ \\
 R L &\rightarrow R L \\
 R L &\rightarrow L R \\
 L R &\rightarrow R L \\
 L R &\rightarrow L R
 \end{aligned} \tag{6.7}$$

Charge conjugation & flavour universality

We can further halve the number of distinct amplitudes we need to explicitly calculate. Complex conjugation of an initial state vertex gives us a final state vertex

$$\left[\begin{array}{c} e_L^+(P_2) \\ \nearrow \\ \text{---} \\ \searrow \\ e_R^-(P_1) \end{array} = v_L^\dagger(P_2) \sigma^\mu u_R(P_1) \right]^* = u_R^\dagger(P_1) \sigma^\mu v_L(P_2) = \begin{array}{c} e_L^-(P_2) \\ \nearrow \\ \text{---} \\ \searrow \\ e_R^+(P_1) \end{array} \tag{6.8}$$

This means complex conjugation of an amplitude \mathcal{A}^* swaps initial with final states and inverts their charge. Moreover, the photon interacts identically to electrons and muons i.e. **QED respects flavour universality**, so we are free to exchange flavour labels $e \leftrightarrow \mu$ and the amplitude remains the same. These two facts mean we can write these equalities

$$\mathcal{A}^* (e_R^- e_L^+ \rightarrow \mu_R^- \mu_L^+) = \mathcal{A} (\mu_L^- \mu_R^+ \rightarrow e_L^- e_R^+) \stackrel{e \leftrightarrow \mu}{=} \mathcal{A} (e_L^- e_R^+ \rightarrow \mu_L^- \mu_R^+). \tag{6.9}$$

Given the final cross-section is always the modulus square of the amplitude $\sigma \propto \mathcal{A}^* \mathcal{A} = |\mathcal{A}|^2$, these equalities imply we can reduce our problem to only having two distinct amplitudes to evaluate:

$$|\mathcal{A}_{RL \rightarrow RL}|^2 = |\mathcal{A}_{LR \rightarrow LR}|^2, \tag{6.10}$$

$$|\mathcal{A}_{LR \rightarrow RL}|^2 = |\mathcal{A}_{RL \rightarrow LR}|^2. \tag{6.11}$$

Calculating spinor currents

Let us take the negatively (positively) charged particle as having momentum pointing $+\mathbf{p}$ ($-\mathbf{p}$). After all these simplifications, we are left with only having to calculate two combina-

tions

$$\begin{array}{ll} \ell_{\mathbf{p}}^- \ell_{-\mathbf{p}}^+ & \text{Calculate} \\ \text{R L} & v_{\text{L}}^\dagger \boldsymbol{\sigma}^\mu u_{\text{R}} \end{array} \quad (6.12)$$

$$\begin{array}{ll} \text{L R} & v_{\text{R}}^\dagger \bar{\boldsymbol{\sigma}}^\mu u_{\text{L}} \end{array} \quad (6.13)$$

With the initial states are aligned along the the z axis, the vector \mathbf{p} points $(\theta, \varphi) = (0, 0)$ in spherical coordinates. To obtain $\mathbf{p} \rightarrow -\mathbf{p}$, we invert through the origin (called a parity transformation), which implies $\theta \rightarrow \pi - \theta, \varphi \rightarrow \varphi + \pi$, so the $-\mathbf{p}$ vector points $(\theta, \varphi) = (\pi, \pi)$. We insert this into eq. (3.86) to evaluate the spinors

$$u_{\text{R}}(\mathbf{p}) = \sqrt{2E} \begin{pmatrix} 1 \\ 0 \end{pmatrix}, \quad v_{\text{L}}(-\mathbf{p}) = \sqrt{2E} \begin{pmatrix} 0 \\ i \end{pmatrix}, \quad (6.14)$$

$$u_{\text{L}}(\mathbf{p}) = \sqrt{2E} \begin{pmatrix} 0 \\ -1 \end{pmatrix}, \quad v_{\text{R}}(-\mathbf{p}) = \sqrt{2E} \begin{pmatrix} -i \\ 0 \end{pmatrix}. \quad (6.15)$$

For each of the four components we have to evaluate the action of the Pauli matrices on the spinors for each of the four vector components equation (3.50):

$$v_{\text{L}}^\dagger \boldsymbol{\sigma}^\mu u_{\text{R}} = 2E \begin{pmatrix} 0 & -i \\ I & \boldsymbol{\sigma} \end{pmatrix} \begin{pmatrix} 1 \\ 0 \end{pmatrix} = 2E \begin{pmatrix} 0 \\ -i \\ 1 \\ 0 \end{pmatrix}, \quad (6.16)$$

$$v_{\text{R}}^\dagger \bar{\boldsymbol{\sigma}}^\mu u_{\text{L}} = 2E \begin{pmatrix} I & 0 \\ -\boldsymbol{\sigma} & \end{pmatrix} \begin{pmatrix} 0 \\ -1 \end{pmatrix} = 2E \begin{pmatrix} 0 \\ i \\ 1 \\ 0 \end{pmatrix}. \quad (6.17)$$

Interestingly, this is precisely proportional to the two independent (circular) polarisation states of the photon $\boldsymbol{\varepsilon}_\mu^\circ, \boldsymbol{\varepsilon}_\mu^\ominus$ that we learn in the classical theory of electromagnetic waves.

The final-state $\mu^- \mu^+$ pair cannot be created with any preferred direction φ in the x - y plane (the two 3-momentum vectors must sum to zero) because the initial state $e^- e^+$ had no overall linear momentum in the x - y plane. Nonetheless, we let the $\mu^- \mu^+$ pair have any θ and account for these possibilities by rotating the $\mu^- \mu^+$ vector in the x - z plane via the rotation matrix R_θ :

$$R_\theta \left[v_{\text{L}}^\dagger \boldsymbol{\sigma}^\mu u_{\text{R}} \right] = \begin{pmatrix} 1 & 0 & 0 & 0 \\ 0 & \cos \theta & 0 & \sin \theta \\ 0 & 0 & 1 & 0 \\ 0 & -\sin \theta & 0 & \cos \theta \end{pmatrix} \begin{pmatrix} 0 \\ -i \\ 1 \\ 0 \end{pmatrix} = \begin{pmatrix} 0 \\ -i \cos \theta \\ 1 \\ i \sin \theta \end{pmatrix} \quad (6.18)$$

6.2 Scattering amplitude and cross-section

Finally putting it all together with the photon propagator $\eta_{\mu\nu}/Q^2$, with $Q^2 = 2E$, this results in a four-vector dot product to obtain the two unique amplitudes:

$$\mathcal{A}_{\text{LR} \rightarrow \text{RL}} = \left[u_{\text{R}}^\dagger \bar{\sigma} v_{\text{L}} \right] \cdot \left[R_\theta v_{\text{L}}^\dagger \sigma u_{\text{R}} \right] = -e^2(1 + \cos \theta), \quad (6.19)$$

$$\mathcal{A}_{\text{RL} \rightarrow \text{RL}} = \left[v_{\text{L}}^\dagger \bar{\sigma} u_{\text{R}} \right] \cdot \left[R_\theta v_{\text{L}}^\dagger \sigma u_{\text{R}} \right] = -e^2(1 - \cos \theta). \quad (6.20)$$

Traditionally, electron-positron accelerators do not collide beams with known polarisation state, so half the time for each electron and positron they are in the L state and the other half R state. Moreover, particle detectors cannot directly measure the spin state of each outgoing muons so we sum over the four non-zero amplitudes. This gives the overall amplitude as:

$$\frac{1}{4} \sum_{\text{spins}} |\mathcal{M}|^2 = \frac{1}{4} \left(2 |e^2(1 + \cos \theta)|^2 + 2 |e^2(1 - \cos \theta)|^2 \right) = e^4(1 + \cos^2 \theta). \quad (6.21)$$

Assembling this in the Fermi golden rule and phase space for two ultrarelativistic particles gives the differential cross-section as a function of $\cos \theta$:

$$\frac{d\sigma(e^-e^+ \rightarrow \mu^-\mu^+)}{d\cos \theta} = \frac{\pi\alpha_{\text{EM}}^2}{2s}(1 + \cos^2 \theta). \quad (6.22)$$

To obtain the total cross-section, integrate over the full range of $\cos \theta$:

$$\sigma = \frac{\pi\alpha_{\text{EM}}^2}{2s} \int_{-1}^1 (d\cos \theta)(1 + \cos^2 \theta), \quad (6.23)$$

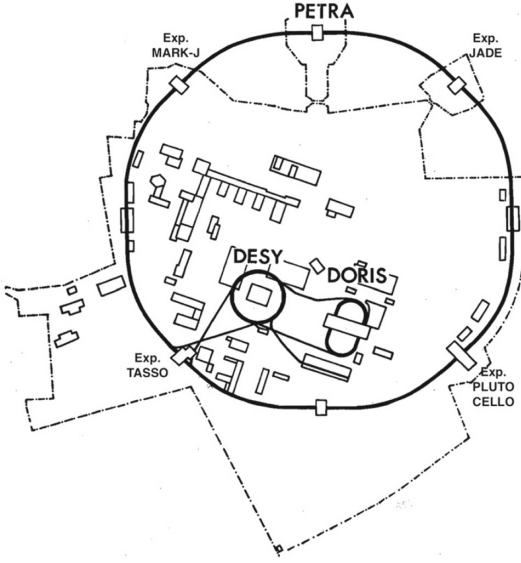
which gives the final result:

$$\sigma(e^-e^+ \rightarrow \mu^-\mu^+) = \frac{4}{3} \frac{\pi\alpha_{\text{EM}}^2}{s}. \quad (6.24)$$

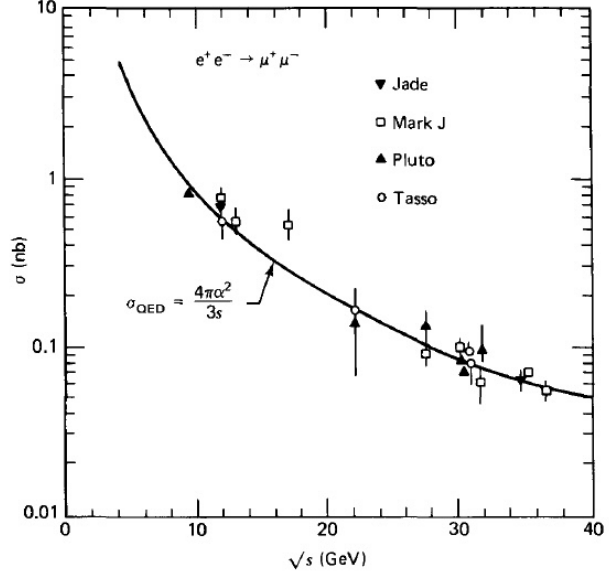
This can be compared with the PETRA accelerator at DESY as precision tests of QED at high energies (figure 34b). At higher-energies, the Z boson resonance exchange becomes important, which is shown later in figure 102 when we discuss electroweak interactions.

6.3 Breit-Wigner resonances

In s-channel annihilation reactions like $e^-e^+ \rightarrow X \rightarrow \mu^-\mu^+$, intermediate resonances with non-zero mass can appear as X such as a Z boson. We can consider reactions of the form $i \rightarrow X \rightarrow f$ with an unstable intermediate state X, which we describe as a Breit-Wigner



(a) PETRA Collider, DESY [47]

(b) $e^-e^+ \rightarrow \mu^-\mu^+$ cross-section vs \sqrt{s} .**Figure 34: PETRA collider tests of QED.** Plot from Hazel and Martin (1984)

resonance. We can write the wave function ψ_t of a state with energy E_0 and lifetime $\tau = 1/\Gamma$ is

$$\psi_t = \psi_0 e^{-iE_0 t} e^{-t/2\tau} = \psi_0 e^{-(iE_0 + \Gamma/2)t}. \quad (6.25)$$

The evolution of ψ_t as a function of time as a function of energy ψ_E is given by the Fourier transform

$$\psi_E = \int e^{-iEt} \psi_t = \psi_0 \int e^{-t[i(E_0 - E) + \Gamma/2]} dt \propto \frac{1}{(E - E_0) - i\Gamma/2} \quad (6.26)$$

The cross-section is then the modulus square $\sigma \propto \psi_E^* \psi_E$ to give the **Breit-Wigner formula**. This describes the cross-section of a reaction $i \rightarrow X \rightarrow f$ in energy E space:

$$\sigma_{i \rightarrow X \rightarrow f} = \frac{\pi}{p_{\text{in}}^2} \frac{\Gamma_i \Gamma_f}{(E - E_X)^2 + (\Gamma/2)^2} \quad (6.27)$$

Multiplying through by $(E + E_X)$ and applying $E \approx E_X = M_X$ when needed, this is often rewritten in a form that makes Lorentz invariance more manifest

$$\sigma_{i \rightarrow X \rightarrow f} = \frac{\pi}{p_{\text{in}}^2} \frac{\Gamma_i \Gamma_f M_X^2}{(s - M_X^2)^2 + (M_X \Gamma/2)^2}. \quad (6.28)$$

This is a useful phenomenological description of observed unstable particles in experiments. Here is a list of useful vocabulary often used to describe decays of particles:

- **Natural width** $\Gamma = 1/\tau$: rate of (decay) reaction is inversely related to the rest lifetime τ , which corresponds to a width in energy units.
- **Decay channels** $X \rightarrow f, f \in \{1, 2, \dots\}$: All the possible final states an unstable state may decay to.
- **Partial widths** Γ_f : the natural width associated with the specific decay channel f .
- **Total width** $\Gamma = \sum_f \Gamma_f$: the sum over all decay channels' partial widths.
- **Branching ratio** $B_f = \Gamma_f/\Gamma$: The proportion of the rate of a particular decay channel to the total rate of decay.
- **Incident momentum** p_{in} , momentum of the incident particle.
- **System energy** $s = E^2$.
- **Resonance mass** M_X : invariant mass of the intermediate resonance.

We can include extra factors accounting for the multiplicity of spins for the resonance state s_X and initial (say two) particles $s_{1,2}$:

$$\sigma_{i \rightarrow X \rightarrow f}^{\text{with spin}} = \frac{2s_X + 1}{(2s_1 + 1)(2s_2 + 1)} \sigma_{i \rightarrow X \rightarrow f}$$

In practice we perform scattering experiments over various system energies E . If an unstable intermediate state X is produced the cross-section (6.27), and thus probability of decaying to final state f , enhances. This increases the number of events of f at the energy E_X corresponding to the rest mass energy $m_X c^2$ of the **resonance state**.

7 Vacuum loop effects

During 1947 in New York City, a pair of landmark experiments performed at Columbia University revealed the vacuum is dynamical, laying the foundations for quantum field theory. No new particles were discovered, yet these results opened a major paradigm shift in physics. Today, their modern incarnations provide among the most precise tests of quantum field theory.

We discuss the experimental manifestations of three classes of one-loop effects in QED (figure 35). This serves as the experimental complement to QFT classes, where you learn the theoretical techniques to calculate loop diagrams. The fundamental problem is that integrating over all internal loop momenta causes divergences. Particle physics textbooks do not always cover experimental tests of QED loop effects, perhaps because they involve atomic physics techniques; nonetheless I found the Bettini textbook has some nice experimental discussion.

7.1 Lamb shift

Solving the hydrogen atom using the Dirac rather than Schrödinger equation shifts the energy levels by a term of order α^2 :

$$E_{n,j} = -\frac{13.6 \text{ eV}}{n^2} \left[1 + \frac{\alpha^2}{n^2} \left(\frac{1}{j+1/2} - \frac{3}{4n} \right) \right]. \quad (7.1)$$

The additional relativistic term is small ($\alpha^2 \approx 1/18700$) compared to the eV scales of the principal energy levels. This represents the correction from the relativistic motion of an

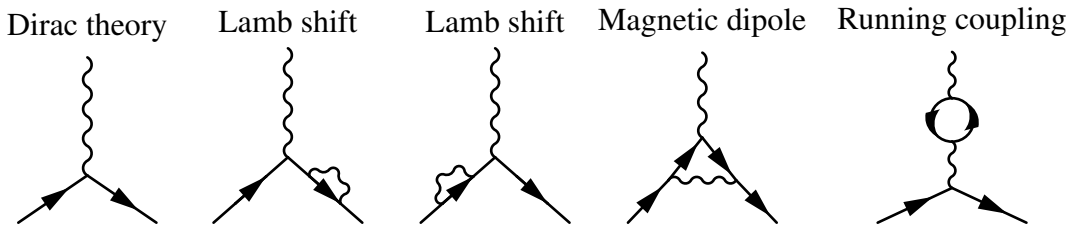


Figure 35: Tree-level (Dirac theory) and one-loop QED diagrams. The Lamb shift arises from the external electron propagators interacting with a photon loop. The anomalous magnetic moment $g - 2$ arises from the electron–photon vertex loop. The running coupling arises from vacuum polarisation inducing an e^+e^- pair loop in the photon propagator.

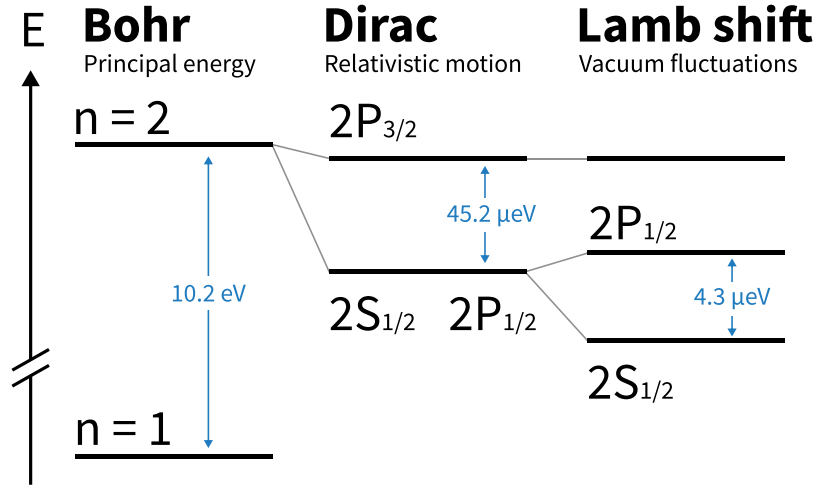


Figure 36: Hydrogen $n = 2$ energy levels. These are sketched for the Bohr model solving the Schrödinger equation with a Coulomb potential, Dirac equation accounting for relativistic electron motion. The electron interacting with fluctuations in the electromagnetic vacuum induces the Lamb shift that splits the $2S_{1/2}$ and $2P_{1/2}$ energy levels otherwise degenerate in the Dirac model.

electron in the Coulomb potential.

A consequence of spin-orbit coupling is that all the $L \neq 0$ states split into e.g. $2P_{1/2}, 2P_{3/2}$, with notation nL_j . But states with the same principal energy level n and total angular momentum j but different orbital L number can have degenerate energies (figure 36). This degeneracy between the $2S_{1/2}$ and $2P_{1/2}$ states is a predicted by Dirac theory:

$$\Delta E_{\text{Dirac}} = E(2S_{1/2}) - E(2P_{1/2}) = 0. \quad (7.2)$$

To test this degeneracy, Willis Lamb and Robert Retherford performed precision microwave measurements of the hydrogen fine structure in 1947 [48].

They utilise the usual Zeeman effect of splitting energy levels by applying a magnetic field to the hydrogen atom. What they measured is shown in figure 38. For nonzero magnetic field $B \neq 0$, they measure energy-level transitions with respect to the reference $2P_{3/2}$ state, where the azimuthal angular momentum states $m = +\frac{3}{2}, +\frac{1}{2}, -\frac{1}{2}$ correspond to the different branches. The dashed line shows the expectation from Dirac theory alone. The measured values have lines drawn that extrapolate to a common value for $B = 0$. There is a clear systematic shift of around a 1000 megacycles per second (megahertz), which was measured (more precisely by 1952) to be

$$\Delta E_{\text{Lamb}} = 1057.8 \pm 0.1 \text{ MHz} = 4.3747 \pm 0.0004 \mu\text{eV}. \quad (7.3)$$

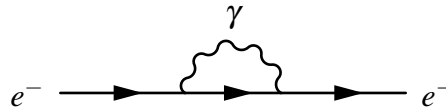


Figure 37: Mass renormalisation loop.

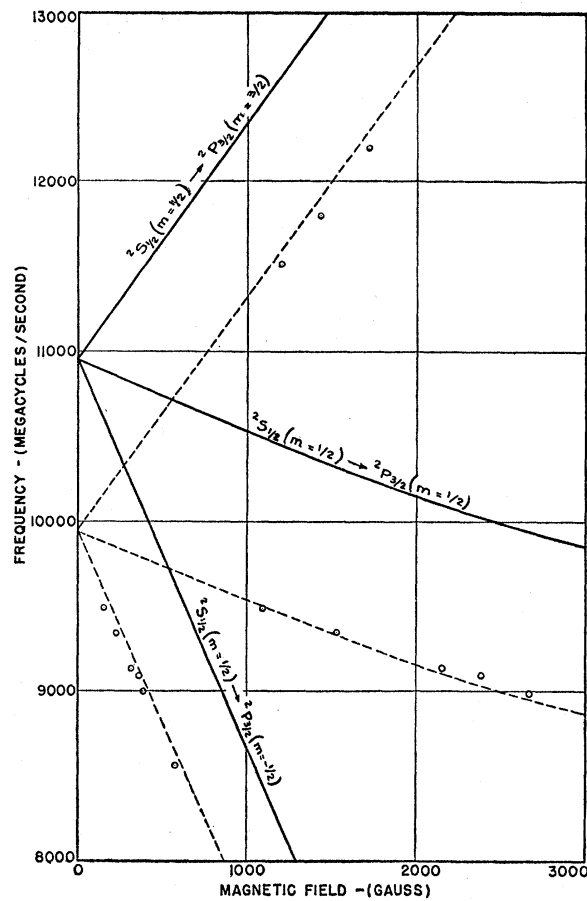


Figure 38: Lamb–Retherford measurement of Lamb shift. Figure: Ref. [48].

This is a watershed moment in physics. It shows that the electromagnetic field is not static, as assumed in classical physics. The field itself is quantum mechanical and therefore exhibits quantum fluctuations, imparting measurable dynamics onto the electron.

7.2 Anomalous magnetic moment

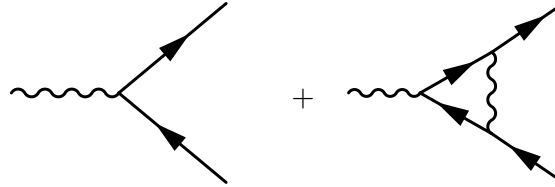
Also working at Columbia in New York, Polykarp Kusch and Henry Foley measured the magnetic moment of the electron to high precision [49, 50]:

$$g_s = 2(1.00119 \pm 0.00005). \quad (7.4)$$

This is the proportionality constant prefixing the Hamiltonian for a magnetic moment in an external field:

$$\mathcal{H} = -\boldsymbol{\mu} \cdot \mathbf{B} = -\frac{g_s e}{2m_f} \mathbf{S} \cdot \mathbf{B}. \quad (7.5)$$

The relevant tree-level and one-loop QED vertex diagrams for the g-factor are:



$$g = 2 + \frac{\alpha}{\pi} \quad (7.6)$$

The value of 2 is predicted by the Dirac equation and the one-loop α/π contribution. This one-loop correction to the QED vertex was first calculated by Julian Schwinger in 1948 [51]:

$$a_e^{1\text{-loop}} = \frac{g_e - 2}{2} = \frac{\alpha}{2\pi} \simeq 0.00116. \quad (7.7)$$

Calculating this is somewhat involved and is taught in an advanced quantum field theory class covering renormalization.

Today, the state-of-the-art experimental and theoretical values are simply astounding. The most accurate value of a_e is measured by an electron cyclotron Penning trap at Northwestern University [2]. The main idea for their direct measurement is that the cyclotron ω_c spin-precession ω_s frequencies are equal for $g = 2$:

$$\boldsymbol{\omega}_c = -\frac{e\mathbf{B}}{\gamma m} \quad \text{cyclotron charged particle in B field,} \quad (7.8)$$

$$\boldsymbol{\omega}_s = -\frac{e\mathbf{B}}{\gamma m} \left[1 + \gamma \left(\frac{g-2}{2} \right) \right] \quad \text{Larmor precession of spin in B field.} \quad (7.9)$$

Their measured differences are therefore approximately related to the anomalous precession frequency $\omega_a \simeq \omega_c - \omega_s \propto g - 2$:

$$\omega_a \simeq \omega_c - \omega_s \propto \frac{g-2}{2} \frac{e}{m} B. \quad (7.10)$$

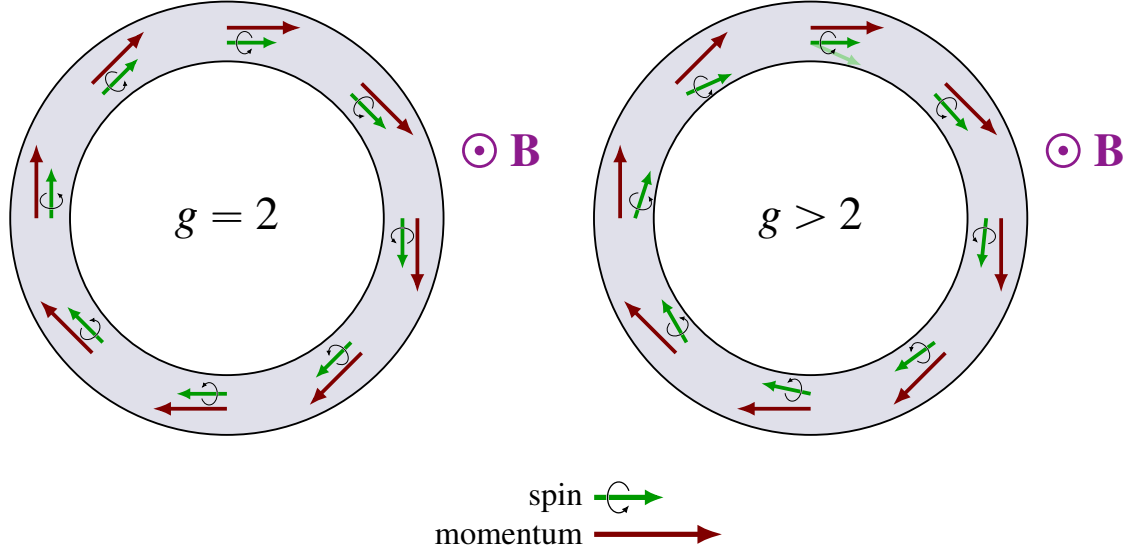


Figure 39: Penning trap spin-precession measurement schematic. This shows the spin precession and momentum vectors for $g = 2$ and $g \neq 2$. Figures: [tikz.net](https://www.tikz.net).

The main experimental aspect that needs to be known very well is the magnetic field B .

This is compared to theory predictions from 10th order QED calculations, which require inputs from fine-structure constant α_{EM} measurements at Paris [3] and Berkeley [52]. The state-of-the-art values are displayed in figure 41 with all the digits spectacularly printed [53]:

$$a_e^{\text{exp}}(\text{cyclotron}) = 0.001\,159\,652\,180\,59\,(13) \quad [2], \quad (7.11)$$

$$a_e^{\text{theory}}\left(\alpha_{\text{EM}}^{\text{Rb}}\right) = 0.001\,159\,652\,182\,037\,(720)_{\alpha_{\text{EM}}^{\text{Rb}}(11)_{\text{theory}}(12)_{\text{hadron}}} \quad [3] \quad (7.12)$$

$$a_e^{\text{theory}}\left(\alpha_{\text{EM}}^{\text{Cs}}\right) = 0.001\,159\,652\,181\,606\,(229)_{\alpha_{\text{EM}}^{\text{Cs}}(11)_{\text{theory}}(12)_{\text{hadron}}} \quad [52]. \quad (7.13)$$

The three parentheses refer to the uncertainties from fine-structure constant measurements (α_{EM}), numerical evaluation of the tenth-order loop calculations (theory), and the hadronic contributions (hadron). At tenth order in α_{EM} , there are 12,672 diagrams correcting the vertex calculations involving mesmerising loop diagrams [54], ten of which are shown in figure 40. Even more remarkably, the dominant uncertainty on these calculations arise from experimental systematic uncertainties in the measurements of the fine-structure constant α_{EM} . The Standard Model does not predict the value of α_{EM} , which is why we must measure it independently.

Fine structure constant measurements are independently performed using the **atomic recoil method** [3, 52]. This measure the recoil velocity $v_{\text{rec}} = \hbar k/M$ of a cold atom with

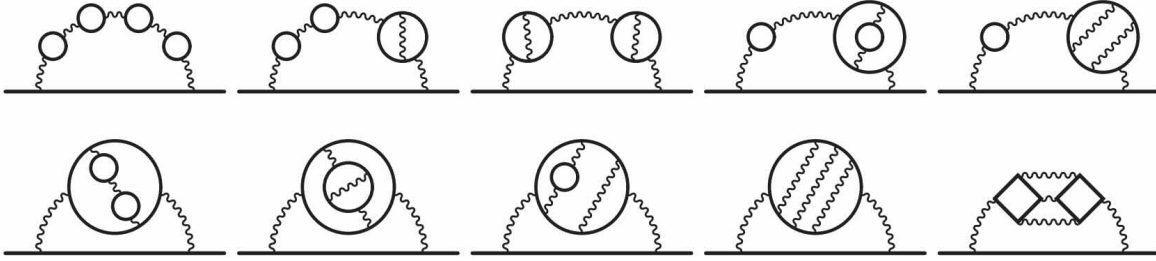


Figure 40: Example digrams from tenth order QED. Image: Ref. [54]

mass M when absorbing a photon with momentum $\hbar k$ from an external laser. This determines the ratio \hbar/M which can be related to the fine structure constant via the Rydberg formula:

$$\alpha_{\text{EM}}^2 = \frac{2R_\infty}{c} \frac{M}{m_e} \frac{h}{M}. \quad (7.14)$$

The prefactors to \hbar/M are known to extraordinary accuracy from CODATA [55]: the Rydberg constant R_∞ is known to parts per trillion (ppt) from hydrogen spectroscopy, while the atom-to-electron mass ratio M/m_e is determined from the relative atomic mass being 69 (30) ppt for rubidium (electron).

Evidently, resolving the tension between the two measurements of α_{EM} made by rubidium and caesium atoms is essential to make progress in testing the Standard Model. Nonetheless, that we are confronting discrepancies at better than parts per trillion is just spectacular for experiment and theory. These are monumental triumphs of scientific inquiry.

7.3 Running coupling

Another profound consequence of quantum field theory is that couplings we initially call ‘constants of nature’ actually depend on the energy at which we measure them. The underlying physical effect is **vacuum polarisation**. The physical picture is that the vacuum around a particle actually polarises i.e. the vacuum is surrounded by a cloud of positive and negative particles (figure 42). These electron-positron ($-+$) pairs are spontaneously created and annihilated from the vacuum as quantum fluctuations. The higher the energy the particle we use to probe another, the more we probe this polarisation. This picture means far away from the electron, we see a lower effective charge because the positive charges cancel out the negative charge of the electron.

But if we accelerate a probe particle with high momentum, this can wade through the cloud of virtual particles and see a higher effective charge. This leads to the notion that the measured electromagnetic coupling increases with momentum transfer due to the existence of

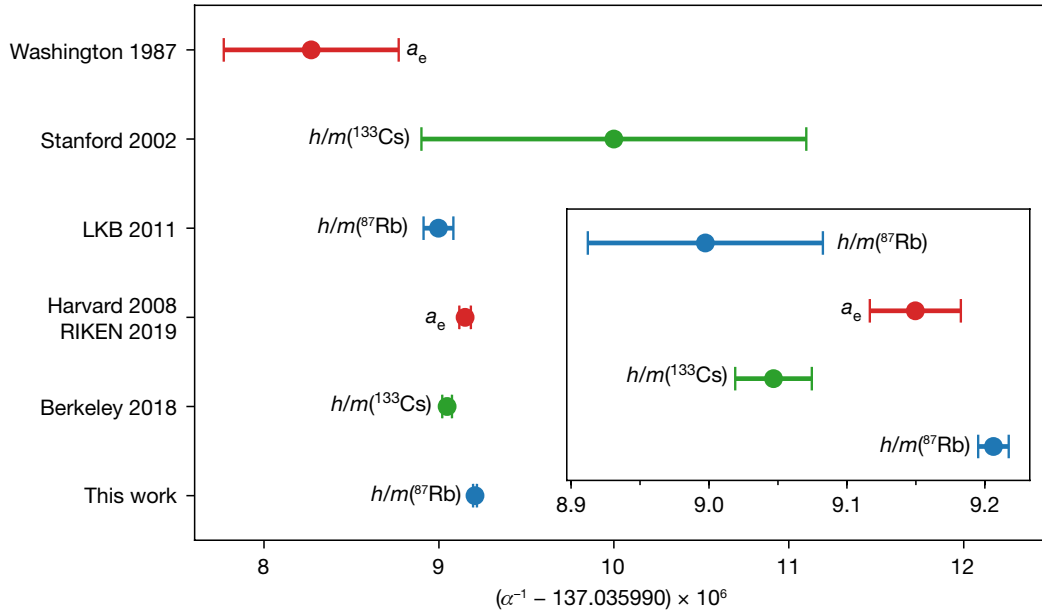


Figure 41: Fine-structure constant measurements. The determination of the fine-structure constant via the matter recoil method (blue and green) compared with Penning trap cyclotron measurements of the electron anomalous magnetic moment a_e (red). Figure: Ref. [3].

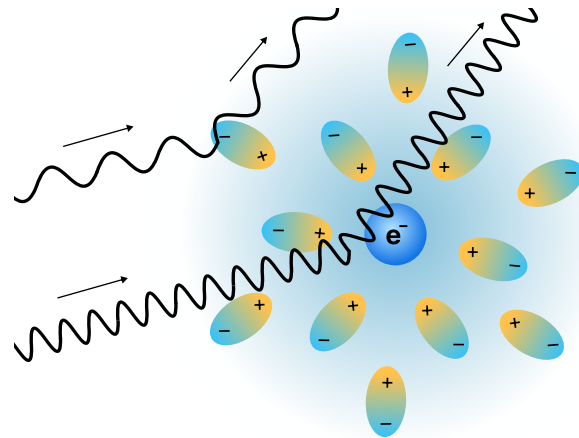


Figure 42: Vacuum polarisation as a cloud of virtual particles. Interactions of a low energy (longer wavelength) particle probing an electron are screened by the cloud, resulting in a smaller measured coupling. A high energy (shorter wavelength) particle can probe deeper into the cloud, resulting in a larger measured coupling.

quantum fluctuations. Specifically, the photon propagator receives corrections from fermion

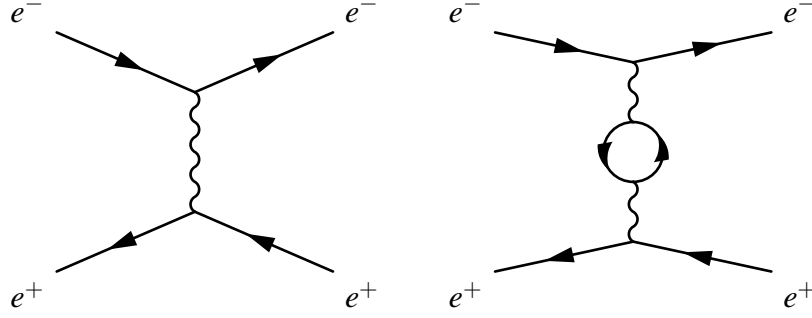


Figure 43: Bhabba scattering. Tree-level (left) and one-loop (right) vacuum polarisation diagrams in t-channel exchange.

loops:

$$\Pi_{\text{meas}} = \text{wavy line} + \text{wavy line with one loop} + \text{wavy line with two loops} + \dots \quad (7.15)$$

We can write the structure of the physical photon propagator Π_{phys} as a perturbative expansion in the bare coupling α_0 and bare photon propagator Π , with each fermion loop contributing a negative sign:

$$\Pi_{\text{phys}} = \Pi + \Pi e(-1)I(q^2)e\Pi_0 + \Pi eI(q^2)e eI(q^2)e\Pi_0 - \dots \quad (7.16)$$

$$= \Pi_0 - \alpha_0 \Pi I(q^2) \Pi + \alpha_0^2 \Pi I(q^2) \Pi I(q^2) \Pi - \dots \quad (7.17)$$

Quantum Field Theory classes teach us how to evaluate loop integral $I(q^2)$. We could look up the result in a textbook [1] to find that the amplitude changes by $1 - I(q^2)$:

$$I(q^2) = \frac{\alpha}{3\pi} \int_{m_e^2}^{\Lambda^2} \frac{dk^2}{k^2} - \frac{2\alpha}{\pi} \int_0^1 dx(1-x) \ln \left[1 - \frac{q^2 x(1-x)}{m_e^2} \right]. \quad (7.18)$$

We shall now sketch the process of renormalisation in a page. The first term of the loop integral is famously infinite when integrating over all momentum k . We admit that we cannot know physics at arbitrarily small distance (or large energy) scales and impose an energy cutoff Λ . At high momentum transfers $q^2 \gg m_e^2$ limit, the integral becomes

$$I(q^2) = \frac{\alpha}{3\pi} \ln \left(\frac{\Lambda^2}{-q^2} \right). \quad (7.19)$$

The perturbative expansion to higher loops orders can be summed as a geometric series $S = 1/(1-r)$:

$$1 - I(q^2) + [I(q^2)]^2 - [I(q^2)]^3 + \dots = \frac{1}{1 + (\alpha/3\pi) \ln(\Lambda^2/Q^2)}, \quad (7.20)$$

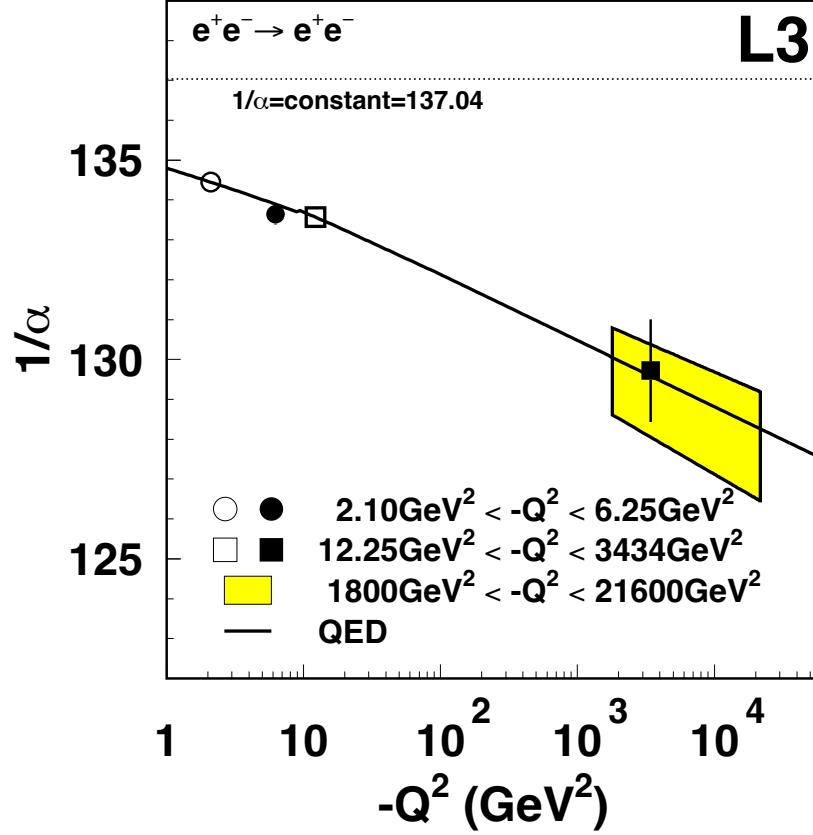


Figure 44: Running electromagnetic coupling. Electromagnetic coupling as a function of momentum transfer squared Q^2 measured by the L3 Experiment.

where we have defined $Q^2 = -q^2$. The net impact of this is a shift in the coupling $\alpha(Q^2)$ constant measured at scale Q^2 relative to the bare coupling constant α_0

$$\alpha(Q^2) = \frac{\alpha_0}{1 + (\alpha_0/3\pi) \ln(\Lambda^2/Q^2)}. \quad (7.21)$$

We can make measurements of $\alpha(Q^2 = \mu^2)$ at a reference mass scale μ (e.g. the electron mass $\mu = m_e$), which allows us eliminate α_0 by subtracting $\alpha^{-1}(Q^2) - \alpha^{-1}(\mu^2)$ to obtain

$$\alpha(Q^2) = \frac{\alpha(\mu^2)}{1 - [\alpha(\mu^2)/3\pi] \ln(Q^2/\mu^2)}. \quad (7.22)$$

This remarkable result shows that by considering only measurable values of $\alpha(Q^2)$, we remove the dependence on the arbitrary cutoff scale Λ . This is the process of **renormalisation** via the cutoff method, and μ is the **renormalisation scale**. The result is that the coupling now depends on the momentum scale Q^2 . The differential equation describing this evolution

is called the **beta function**:

$$\frac{\partial \alpha_{\text{EM}}}{\partial Q} = \beta(\alpha_{\text{EM}}) = \frac{2\alpha_{\text{EM}}^2}{3\pi}. \quad (7.23)$$

Figure 44 shows high-energy electron-positron accelerator measurements of $e^+e^- \rightarrow e^+e^-$ at the L3 Experiment [56]. We can see that measured values at the different energy scales are

$$\alpha_{\text{EM}}(q^2 \rightarrow 0) \simeq \frac{1}{137}, \quad (7.24)$$

$$\alpha_{\text{EM}}(q^2 = m_Z^2) \simeq \frac{1}{128}. \quad (7.25)$$

In quantum electrodynamics, the effective coupling α_{EM} grows with energy scale.